

Sedimentological and palynological records since 10 ka BP along a proximal-distal gradient on the Armorican shelf (NW France)

Ophélie David, Aurélie Penaud, Muriel Vidal, Wiem Fersi, Clément Lambert, Evelyne Goubert, Maiwenn Herlédan, Pierre Stéphan, Yvan Pailler, Jean-François Bourillet, et al.

▶ **To cite this version:**

Ophélie David, Aurélie Penaud, Muriel Vidal, Wiem Fersi, Clément Lambert, et al.. Sedimentological and palynological records since 10 ka BP along a proximal-distal gradient on the Armorican shelf (NW France). Quaternary Science Reviews, 2022, 293, 10.1016/j.quascirev.2022.107678 . insu-03824739

HAL Id: insu-03824739
https://insu.hal.science/insu-03824739

Submitted on 21 Oct 2022

HAL is a multi-disciplinary open access archive for the deposit and dissemination of scientific research documents, whether they are published or not. The documents may come from teaching and research institutions in France or abroad, or from public or private research centers.

L'archive ouverte pluridisciplinaire **HAL**, est destinée au dépôt et à la diffusion de documents scientifiques de niveau recherche, publiés ou non, émanant des établissements d'enseignement et de recherche français ou étrangers, des laboratoires publics ou privés.

Quaternary Science Reviews
October 2022, Volume 293 Pages 107678 (22p.)
https://doi.org/10.1016/j.quascirev.2022.107678
https://archimer.ifremer.fr/doc/00792/90413/

Archimer
https://archimer.ifremer.fr

Sedimentological and palynological records since 10 ka BP along a proximal-distal gradient on the Armorican shelf (NW France)

David Ophélie [1, 2, *], Penaud Aurélie [1], Vidal Muriel [1], Fersi Wiem [1], Lambert Clément [2], Goubert Evelyne [2], Herlédan Maiwenn [3], Stéphan Pierre [4], Pailler Yvan [5], Bourillet Jean-François [6], Baltzer Agnès [7]

[1] Geo-Ocean, Univ. Brest, CNRS, Ifremer, UMR 6538, F-29280 Plouzané, France
[2] Geo-Ocean, Univ. Bretagne Sud, Univ. Brest, CNRS, Ifremer, UMR 6538, F-56000 Vannes, France
[3] Univ. Lille, Laboratoire D'Océanologie et de Géosciences, UMR 8187, F-59655 Villeneuve d'Ascq, France
[4] CNRS, Littoral Environnement Télédétection Géomatique, UMR 6554, IUEM, F-29280 Plouzané, France
[5] Chaire Armerie, Univ. Brest, Inrap, Littoral Environnnement Télédétection Géomatique, UMR 6554, IUEM, F-29280 Plouzané, France
[6] Ifremer, Ressources Physiques et écosystèmes de Fond de Mer, Centre de Bretagne. 1625, Route de Ste Anne, CS 10070, F-29280 Plouzané, France
[7] Univ. Nantes, Laboratoire Géolittomer/IGARUN, UMR 6554, F-44300 Nantes, France

* Corresponding author : Ophéllie David, email address : ophelie.david@univ-ubs.fr

aurelie.penaud@univ-brest.fr ; muriel.vidal@univ-brest.fr ; wiem.fersi@univ-brest.fr ; clement.lambert@univ-ubs.fr ; evelyne.goubert@univ-ubs.fr ; maiwenn.herledan.etu@univ-lille.fr ; pierre.stephan@univ-brest.fr ; yvan.pailler@inrap.fr ; jean.francois.bourillet@ifremer.fr ; agnes.baltzer@univ-nantes.fr

Abstract :

New findings acquired in Armorican shelf (core MD08-3204 CQ: Bay of Quiberon and core VK03-58bis: South Glénan islands) depict Holocene paleoenvironmental changes since 10 ka BP through a multi-proxy dataset including sedimentological and palynological data. First, grain-size analyses and AMS-14C dates show a common sedimentary history for both study cores. The slowdown of the relative sea level (RSL) rise was accompanied by a drop of the sedimentation rates between ~8.3 and 5.7 ka BP; the rates had been relatively higher at the onset of the Holocene. This interval led to the establishment of a shell-condensed level, identified in core VK03-58bis by the "Turritella layer" and interpreted as a marker for the Maximum Flooding Surface. Palynological data (pollen and dinoflagellate cyst assemblages) acquired in core MD08-3204 CQ argue for an amplification of the fluvial influence since 5.7 ka BP; the establishment of the Highstand System Tract (i.e., mixed marine and fluviatile influences on the platform) then accompanied the slowdown of the RSL rise rates. On the shelf, the amplification of Anthropogenic Pollen Indicators (API) has been better detected since 4.2 ka BP, due not only to the increase of human impact but also due to a stronger fluvial influence on the shelf during the Late Holocene. Palynological data, recorded on the 8.5–8.3 ka BP interval along an inshore-offshore gradient, also demonstrate the

Please note that this is an author-produced PDF of an article accepted for publication following peer review. The definitive publisher-authenticated version is available on the publisher Web site.

complexity of the palynological signals such as i) the fluvial influence that promotes some pollen taxa (Alnus and Corylus) from proximal areas and ii) the macro-regionalization of palynomorph sources in distal cores. In addition, the comparison of palynological tracers, including API, over the last 7 kyrs BP, with South Brittany coastal and mid-shelf sites subject to northern vs. southern Loire catchment areas, shows a major hydro-climatic effect on the reconstructed palynological signals. Strengthened subpolar gyre (SPG) dynamics, combined with recurrent positive North Atlantic Oscillation (NAO) configurations, appear responsible for increased winter precipitation and fluvial discharge over northern Europe, as in Brittany. Conversely, weakened SPG intervals, associated with recurrent negative NAO-like modes, are characterized by intensified winter fluvial discharge over southern Europe. Interestingly, at an infra-orbital timescale, we record major peaks of API during periods of strengthened (/weakened) SPG dynamics in sites subject to detritic-organic matter inputs from Brittany (/Loire) watersheds.

Highlights

► The Armorican shelf sedimentation reflects the Holocene relative sea level rise. ► The condensed "*Turritella* layer" testifies of the Maximum Flooding Surface. ► Distortion of palynological signals from proximal to distal environments. ► The hydro-climatic forcing affects the anthropogenic pollen signal in shelf sediments. ► The Bronze and Middle Ages are recorded as main steps in human activity increase.

Keywords : Holocene, South Brittany, Pollen, Dinoflagellate cysts, Paleoenvironmental changes, Turritella layer, Anthropogenic pollen indicators (API), Fluvial discharge

Please note that this is an author-produced PDF of an article accepted for publication following peer review. The definitive publisher-authenticated version is available on the publisher Web site.

1. Introduction

The Holocene (i.e., the last 11.7 kyrs BP) is characterized by climate variability operating differently according to timescales. In the first instance, the summer insolation at 65°N gradually decreases during the Holocene and induces a drop in Northern Hemisphere summer air temperatures (*Berger and Loutre, 1991*) fostering the Mid-Holocene freshening and the increase in winter precipitation over Northwestern (NW) Europe (e.g., *Morzadec-Kerfourn, 1974*; *Naughton et al., 2007*; *Penaud et al., 2020*). Superimposed on the long-term Holocene climate trend, millennial-scale abrupt climate events derive from repeated cryospheric instabilities (i.e., Bond events, *Bond et al., 1997*; or Rapid Climate Changes with a more global-scale perspective, *Mayewski et al., 2004*). Over Europe, the infra-orbital Holocene climate subsequently oscillates at multidecadal timescales and is mainly driven by North Atlantic Oscillation-like (NAO; e.g., *Hurrell, 1995*; *Hurrel et al., 2003*) varying atmospheric regimes (e.g., *Olsen et al., 2012*; *Morley et al., 2014*) and North Atlantic Ocean gyre dynamics (e.g., *Hátún et al., 2005*; *Thornalley et al., 2009*; *Moffa-Sánchez and Hall, 2017*; *Penaud et al., 2020*; *Lambert et al., 2020*).

Following the deglaciation, the Early Holocene is also characterized by high Relative Sea Level (RSL) rise rates that decreased during the Mid to Late Holocene along the Atlantic coasts (e.g., Caribbean region and South America, *Milne et al., 2005*; Southern Bay of Biscay; *Leorri et al., 2012a, b*; North-America, *Engelhart et al., 2015*; Europe, *García-Artola et al., 2018*). The RSL evolution is strongly controlled by meltwater inputs and isostatic adjustments, inducing different sea-level rates according to the regions investigated (*Leorri et al., 2012a, b*; *Goslin et al., 2015*; *García-Artola, 2018*). Along the southern Brittany coasts (*García-Artola et al., 2018*), the RSL rose rapidly between 20 ka BP (~ -25 m) and ~7 ka BP (~ -5 m) and subsequently slowed down at ~6 ka BP (*Goslin et al., 2015*; *Stéphan et al., 2015*; *García-Artola et al., 2018*), leading to the development of tidal flats in estuarine environments and saltmarshes

along the European coasts (e.g., *Joly and Visset, 2009*; *Menier et al., 2010*; *Stéphan et al., 2019*; *Penaud et al., 2020*). The Holocene marine transgression thus progressively flooded fluvial paleovalleys, resulting in the geomorphological transformation of French Atlantic coastal ecosystems (e.g., *Proust et al., 2001*; *Weber et al., 2004*; *Chaumillon et al., 2008*; *Menier, 2004*; *Menier et al., 2010*; *Baltzer et al., 2014*; *Gregoire et al., 2017)*.

Superimposed on these natural forcings, Holocene paleoenvironments are impacted by the evolution of human societies (i.e., cultural and technical changes), especially since the start of the Neolithic (i.e., ~7 ka BP in Brittany; *Pailler et al., 2008*). The related landscape changes are mainly recorded thanks to palynological data highlighting the progressive deforestation and the introduction and intensification of the agro-pastoral activities thanks to Anthropogenic Pollen Indicators (API) (e.g., *Marguerie, 1992*; *Visset et al., 1995, 1996*; *Gaudin, 2004*; *Visset and Bernard, 2006*; *Naughton et al., 2007*; *Fernane et al., 2014, 2015*; *Penaud et al., 2020*). In parallel with terrestrial bio-indicators (pollen grains), aquatic bio-indicators (dinoflagellate cysts or dinocyts) allow discussing surface water evolution through time linked with sea level variations or leaching of nutrients from soils to coastal waters (e.g., *Lambert et al., 2018*; *Penaud et al., 2020*). These latter paleoceanographic tracers are found in worldwide sediments and their distribution are mainly driven by sea-surface parameters (i.e., temperature, salinity), nutrient concentration and primary productivity regimes, as well as inshore-offshore gradients (e.g., *Zonneveld et al., 2013*; Van *Nieuwenhove et al., 2020*; *Marret et al., 2020*; *de Vernal et al., 2020*). Along the Brittany coasts, the modern distribution of dinocysts has recently been updated (*Ganne et al., 2016*; *Lambert et al. 2017, 2022*). Furthermore, *Penaud et al. (2020)* have recently classified dinocyst taxa into ecological groups according to different bathymetric contexts (i.e., estuarine, shallow bay, inner neritic, outer neritic, full oceanic) along a marine (distal or offshore) to coastal (proximal) temporal transect across the Bay of Biscay.

The Armorican shelf, subject to both fluvial (i.e., mainly the Loire and Vilaine rivers) and oceanic (i.e., North Atlantic Ocean through gyre dynamics) influences (Fig. 1a), is a key area for conducting paleoenvironmental studies (*Naughton et al., 2007*; *Penaud et al., 2020*). In this study, we examine two cores retrieved in the Armorican shelf (Figs. 1a, b): cores MD08-3204 CQ (Bay of Quiberon) and VK03-58bis (Grande Vasière, South Glénan sector). Previous studies conducted on core VK03-58bis aimed at discussing the sedimentological structure of the Grande Vasière (*Folliot, 2004*; *Bourillet et al., 2005, 2006)* as well as landscape-climate changes in northwestern France (*Naughton et al., 2007)*. Core MD08-3204 CQ was previously examined by *Baltzer et al. (2014)* to reconstruct the sedimentary filling of the Bay of Quiberon. The present work is based on i) new radiocarbon dates obtained for both studied cores and ii) new palynological (pollen and dinocyst) analyses conducted on core MD08-3204 CQ. Our first objective is to refine the chronostratigraphy of both sequences to reconstruct the sedimentary dynamics on the shelf in relation with the long-term evolution of the RSL rise. This allows providing a new stratigraphical significance for the "*Turritella* layer", an interval characterized by a high concentration of *Turritella* communis shells in core VK03-58bis (*Folliot, 2004*; *Bourillet et al., 2005, 2006*; *Naughton et al., 2007*; *Baltzer et al., 2015*). Secondly, this study aims at understanding palynological signatures along a proximal-distal gradient from coastal (*Lambert et al., 2019*; this study), mid-shelf (*Naughton et al., 2007*) to deep marine environments (*Zumaque et al., 2017*; *Fersi et al., in prep*) on the 8.5–8.3 ka BP interval. Finally, the API detection is discussed from continental (South Brittany maritime marsh; *Fernane et al., 2015*) to Armorican shelf environments (*Penaud et al., 2020*; this study) over the last 7 kyrs BP taking into account anthropogenic and natural forcing.

2. Environmental context

2.1. Hydrographical context of the Bay of Biscay

The study area extends from the northern part of the Bay of Biscay (BoB), an open oceanic basin in the north-eastern Atlantic Ocean, to the coastal zone of South Brittany. In the BoB, modern residual shelf currents (Fig. 1a) depend on wind-driven, tidally-induced, and density-driven flows (*Pingree and Le Cann, 1989*; *Koutsikopoulos and Le Cann, 1996*; *Castaing et al., 1999*). Currently, seasonal atmospheric dynamics (*Pingree and Le Cann, 1989*) and river discharge (*Lazure and Jégou, 1998*; *Lazure et al., 2008*) lead to the complex hydrological system presented in *Charria et al. (2013)*. In winter (i.e., October to March), a SW-dominant wind regime forces a SE to NW shelf current as schematized in Fig. 1a, while in summer (i.e., April to September), a NE-dominant wind regime forces a NW to SE shelf current (*Charria et al., 2013*; *Charria, 2018*). From mid-autumn to early spring, freshwater discharge of the Loire and Gironde rivers (i.e., values greater than 1500 m^3/s; *Castaing and Allen, 1981*) are pushed back toward the BoB coastal areas under the influence of sustained wind activity (Fig. 1a). This leads to a salinity decrease and a sea-surface cooling between the coast and the 100 m isobath. Under increasing winter fluvial discharge, the establishment of the resulting modern "winter horizontal thermohaline front" then characterizes the pronounced disconnection of oceanic and shelf waters (*Castaing et al., 1999*; *Costoya et al., 2016*; Fig. 1a), identified from 3.3 ka BP on the mid-shelf (*Mojtahid et al., 2019*; *Penaud et al., 2020*).

2.2. Sedimentological context of the Armorican shelf

2.2.1. The Bay of Quiberon (BQ)

The Bay of Quiberon (BQ; 4 to 14 km width) is located in the internal domain of the Armorican shelf, between the coast and the 50 m isobath (Figs. 1a, b). This shallow internal domain is

divided into two sectors separated by large paleovalley networks and weakly incised (*Guilcher, 1948*; *Vanney, 1977*; *Menier, 2004*; *Menier et al., 2010, 2014*): i) the inshore region with water depths below 25 m (i.e., bays of Quiberon and Vilaine; Fig. 1b) and ii) the offshore region formed by rocky shoals (i.e., islands of Houat and Hoëdic; Fig. 1b). In the BQ, modern sedimentation consists of fine terrigenous sediments (i.e., muddy sand; Fig. 1b), coming mainly from the swells-driven resuspension of the fine sediments deposited in the Vilaine Bay and from the Morbihan Gulf, Vilaine and Loire river plumes (*Menier et al., 2010, 2014*).

The Holocene sedimentary infilling of the BQ, following the Last Glacial Maximum (~20 ka BP) when the BQ was completely submerged, has been thoroughly studied using seismic profiles and sedimentological analyses (*Baltzer et al., 2014*). The BQ post-glacial flooding was initially confined to paleovalleys, gradually filled by fluvial deposits, which evolved to a subtidal bay (Unit 2 in *Baltzer et al., 2014*). Next, marine deposits indicative of energetic conditions (e.g., sparse marine shell debris, clayey- and sandy-rich deposits) settled during the rapid sea-level rise (8.7 to 6–5 ka BP; Unit 3 in *Baltzer et al., 2014*) until reaching the Maximum Flooding Surface (MFS). Following the RSL rise, BQ sedimentation now reflects highstand sea level conditions established since ~6–5 ka BP (Unit 4 in *Baltzer et al., 2014*).

2.2.2. The Grande Vasière mid-shelf belt (GV)

The Grande Vasière (GV; 225 km length; 40 km wide; surface of 8,000 km²; Fig. 1a), located between 80 and 110 m water depth, is a mid-depth mud belt (*McCave, 1972*; *Dubrulle et al., 2007*). The GV generally designates the upper part of the Holocene sediment accumulation built up at a rate of 0.1 to 0.2 cm/yr (*Lesueur et al., 2001*). The GV consists of a thin layer of silty mud, mainly tens of centimeters thick except on the NNW and SSE edges, overlying two sandy units (*Andreieff et al., 1971*; *Bourillet et al., 2006*). Present-day sediment inputs come from the

winter fluvial terrigenous supply (1.5 10^6 t/yr from the Gironde, 0.5 10^6 t/yr from the Loire, and 0.1 10^6 t/yr from the Vilaine; *Jouanneau et al., 1999*) and the wave erosion (storminess and distant swell) of the NW French coast between April and September (*Jouanneau et al., 1999*; *Dubrulle et al., 2007*). In the BoB, the winter horizontal thermohaline front derives from the extension of winter fluvial turbid plumes up to the 100 m isobath (*Costoya et al., 2016*), explaining the extension of the mid-shelf sediment deposits on the GV (*Castaing et al., 1999*). The provisional sedimentary budget over the last 30 years shows a decrease of the clayey fraction due to the fine material remobilization because of storms and fishing activities (*Bourillet et al., 2006*).

In the northern part of the BoB, the Loire and Vilaine rivers together represent 95% of BoB watersheds. Up to 90% of the nutrient contribution in the northern part of the Armorican shelf comes from the Loire and Vilaine rivers and the southern Brittany coastal river discharge make smaller secondary contributions (*Guillaud et al., 2008*). The northernmost sector of the GV (southwest of Glénan islands; Fig. 1b) is characterized by a thicker, muddy layer, of a few meters of Holocene silty-clayey sediments (*Bourillet et al., 2006*). In this area, a characteristic acoustic reflector in seismic profiles has been identified and attributed to the presence of a remarkable concentration of *Turritella communis* shells, described as the "*Turritella* layer" in the core VK03-58bis (*Folliot, 2004*; *Bourillet et al., 2005, 2006*). The environmental changes required for the establishment of this shell deposit, observed on the Armorican shelf but also elsewhere in the northern Atlantic Ocean (Scottish fjords; *Baltzer et al., 2015*), are still debated.

3. Material and methods

3.1. Studied cores

The CALYPSO square (CASQ) core MD08-3204 CQ (47°30'27.6''N; 3°1'18.6''O; 17 m deep; 8.91 m long) was collected in the central part of the BQ (Figs. 1a, b) onboard the R/V Marion Dufresne in 2008 (MD169/MICROSYSTEMS cruise; *Blamart et al., 2008*). Only the three upper meters are examined in this study.

The VK03-58bis core (47°36.349'N; 4°08.173'W; 96.8 m deep; 2.72 m long) was collected with a vibrocorer, in the NNW edge of the GV off the South Glénan islands (GV; Figs. 1a, b) during the Vibarmor cruise, onboard the R/V *Côtes de la Manche* (*Le Roy, 2003*; '*Défi Golfe de Gascogne*' 2001-2005, Ifremer). The latter sedimentary archive retrieves the totality of the northern GV sediment accumulation (*Bourillet et al., 2005, 2006*; *Naughton et al., 2007*).

3.2. Chronological frameworks

New chronostratigraphies established on both studied cores were used to discuss the sedimentation dynamics on the Armorican shelf. In this study, 11 new AMS-^{14}C dates were obtained for the upper three meters of core MD08-3204 CQ, these were used to build a robust chronostratigraphy based on a total of 15 AMS-^{14}C dates between 287 and 20 cm (Table 1). Regarding core VK03-58bis, 10 additional AMS-^{14}C dates were newly acquired (8 on benthic foraminifera and 2 on *Turritella communis* shells), complementing the 5 earlier AMS-^{14}C dates published in *Naughton et al. (2007)* (Table 2). All AMS-^{14}C dates were calibrated with the CALIB 7.1 software using the IntCal20 calibration curve (*Stuiver and Reimer, 1993*; *Reimer et al., 2020*), first considering a reservoir age of -400 ± 45 years to radiocarbon dates (point 1559 for the lower Loire in the marine20 database; *Tisnérat-Laborde et al., 2010*) for both studied cores (Tables 1 and 2).

Also, this study aims at understanding palynological signatures along a proximal-distal gradient on the Armorican shelf since the subsequent RSL slowdown at ~6 ka BP. For this purpose, an age model was established on the top core section (134–20 cm) of core MD08-3204 CQ using the rbacon package (*Blaauw and Christen, 2011*) in R version 4.1.2 (R Development Core Team, 2021; http://www.r-project.org/). This allowed reconstructing the last 5.7 kyrs BP (Fig. 2a), while no age model was established for the lower section of the core (287–134 cm) because of the peculiar sedimentological context discussed later in the manuscript (i.e., period of remobilization or no sediment deposition). The palynological records obtained on core MD08-3204 CQ were also compared with published palynological datasets from continental (core GL3, Loc'h of Guidel; *Fernane et al., 2015*) and mid-shelf (core CBT-CS11, Grande Vasière, Penmarc'h sector; *Penaud et al., 2020*) sedimentary archives (Figs. 1a, b). For the last two cited cores, all AMS-14C dates previously acquired were re-calibrated and their age models were modified using the same chronological methodologies as the one described for core MD08-3204 CQ (Fig. 2b).

3.3. Sedimentological analyses

In this study, the logs previously established for cores MD08-3204 CQ (*Baltzer et al., 2014)* and VK03-58bis (*Folliot, 2004*) were reviewed thanks to a refined description of the sedimentary facies (Figs. 3 a, b).

Regarding core MD08-3204 CQ, the sedimentological data presented in this study refer to the 299–1 cm section also investigated for palynological data. Sedimentological analyses previously carried out on this core (*Baltzer et al., 2014*) include a sedimentological description and total grain-size analyses (after removal of the organic matter) using a Beckman-Coulter LS230 laser particle analyzer. Also, new calcimetry (% $CaCO_3$; Fig. 3a) and Total Organic Carbon (% TOC; Fig. 3a) data were acquired (UMR 6249 Chrono-environnement laboratory,

Univ. Bourgogne Franche-Comté) thanks to the standard Loss On Ignition (LOI) method (*Heiri et al., 2001*). Sediments were dried at 105°C during 20 hours and then cooled in a dessicator before burning. After weighing, samples were burned at 550°C during 5 hours and weighed to calculate the TOC content. Then, the samples were burned at 950°C during 2 hours and weighed to calculate the carbonate content.

Regarding the VK03-58bis core, new $CaCO_3$-free grain-size analyses (after HCl 30% treatment) were performed on a Malvern Hydro 2000 particle size analyzer (Univ. Bretagne Sud, Pontivy), and added information on previous sedimentological data including grain-size analyses on the total sediment fraction (*Bourillet et al., 2005*; *Naughton et al., 2007*; Fig. 3b). Grain-size statistics for both study cores, including median grain-size (D50) values, were obtained using the GRADISTAT v 8.0 software (*Blott and Pye, 2001*).

3.4. Palynological analyses

New palynological data were acquired on core MD08-3204 CQ (BQ; Fig. 1b) for the upper three meters of the core. A total of 61 samples were taken every 10–20 cm, in the lower part of the sequence (i.e., 290–140 cm), and every ~3 cm in the upper part (i.e., 140–10 cm) within a 1 cm sample (i.e., corresponding to ~2 cm^3).

Palynological treatments on the <150 µm sediment fraction were carried out at the Geo-Ocean laboratory (Univ. Bretagne Occidentale, Plouzané) following the procedure described by *de Vernal et al. (1999)*. First, carbonate and siliceous fractions were removed using chemical treatments (cold 10-25-50% HCl and cold 40-70% HF). Then, mineral clayey fractions were sieved with 10 µm mesh size nylon screens. An optical microscope Leica DMC 2500 at ×630 magnification was used for palynomorph determination, following *Beug (1961)* and *Reille (1995)* for pollen and *Rochon et al. (1999)* and *Van Nieuwenhove et al. (2020)* for dinocyst

identifications. For each sample a minimum of i) 300 pollen grains (150 grains excluding *Pinus* and indeterminate grains; *Fatela and Taborda, 2002*) and ii) 300 dinocysts (100 specimens besides the dominant species *Lingulodinium machaerophorum)*, were counted to systematically ensure statistically reliable assemblages (*Mertens et al., 2009*). Palynological results were then represented in absolute (number of specimens/cm^3) and relative (percentages) abundances (Table 3). Palynological diagrams and cluster analyses were performed using the Psimpoll program (*Bennet, 1992*), and ecological indexes (number of taxa per sample, Margalef diversity, and dominance; Table 3) were calculated using the Past program v 1.75b (*Hammer et al., 2001*). The dinocyst and pollen identified in core MD08-3204 CQ are grouping according to their ecological affinities (see Table 3).

4. Results

4.1. Sediment facies description and chrono-stratigraphical model

4.1.1. The MD08-3204 CQ core: the inshore domain of the Bay of Quiberon

The age-depth plot (Fig. 3a) defines three main stratigraphical intervals. In the lower part, between 299–196 cm, a short time interval encompassing 200 years (8.5–8.3 ka BP) is characterized by high sedimentation rates of about 4.5 mm/yr. Between 196–134 cm (8.3–5.7 ka BP), a drop in sedimentation rates (decreasing to ~0.2 mm/yr), associated with a reversed date, suggests a period of remobilization or no sediment deposition (grey band in Fig. 3a). From 134 cm (5.7 ka BP) to the top of the core, a resumption of lower and constant sedimentation rates of about 0.24 mm/yr is calculated.

Regarding grain-size analyses performed on the total sediment fraction, in the lower part of the core between 299–250 cm, sediments consist of fine to medium sands, with less than 40% of silty-clayey sediments (Fig. 3a). Between 250–200 cm, a larger proportion of silty-clayey sediments (~60% of the grain size distribution) is characterized by an increase of the TOC (higher than 6%; Fig. 3a). Between 200–180 cm, marking the base of the low sedimentation rate interval, total sediment D50 values rise (~40 µm before limit 1 and 150 µm after this limit; Fig. 3a) and correspond to the increase of the proportion of fine to sands. From 180 cm, sediments consist in very fine-sandy (~60% of the grain size distribution, limit 2 in Fig. 3a). Finally, at 134 cm (i.e., limit 3 corresponds to the resumption of constant sedimentation rates), total sediment D50 values decrease (~95 µm before limit 3 and 42 µm after; Fig. 3a). At the same time, both calcimetry (4% before 134 cm and 12% after limit 3) and TOC (lower than 6% before 134 cm and between 6-12% after limit 3) increase.

4.1.2. The VK03-58bis core in the mid-shelf mud belt (northern Grande Vasière)

The age-depth plot of core VK03-58bis (Fig. 3b) defines three main stratigraphical intervals, as for core MD08-3204 CQ. The lower part, between 266–165 cm (10–8.4 ka BP), is characterized by higher sedimentation rates of about 0.6 mm/yr. Between 165–140 cm (8.4–6.3 ka BP), an abrupt drop in sedimentation rates is observed (decreasing to 0.01 mm/yr; grey band in Fig. 3b). From 137 cm (6.3 ka BP) to the top of the core, a resumption of lower sedimentation rates of about 0.22 mm/yr is reconstructed, with values close to the ones calculated for the post-5.7 ka BP interval described for core MD08-3204 CQ (Fig. 3a).

Regarding grain-size analyses performed on the total sediment fraction, during the interval characterized by higher sedimentation rates (~0.6 mm/yr; Fig. 3b), sediments consist mainly of coarser silty sediments with clast debris whose sizes gradually decrease between 270–210 cm. Between ~210–170 cm (Fig. 3b), finer sediments are characterized by decreases of both $CaCO_3$-free and total sediment D50 values. In addition, the interval characterized by a drop in sedimentation rates (~0.01 mm/yr; grey band in Fig. 3b), encompassing a remarkable 161–149 cm level of *Turritella communis*, is marked by a rise of $CaCO_3$-free and total sediment D50 values (~18 µm before limit 1', and 30 µm after this limit). From the first appearance of *T. communis* at 213 cm, their shell concentration gradually increases until reaching the high concentrated level, known as the "*Turritella* layer" (TL; *Bourillet et al., 2005*; *Naughton et al., 2007*; *Baltzer et al., 2015*), visible on the X-Ray radiography (*Bourillet et al., 2005*; Fig. 3b). A few *Turritella* shells, highly scattered, still occur above the TL horizon. From 140 cm onward, corresponding to the resumption of constant sedimentation rates of about 0.22 mm/yr (limit 2'; Fig. 3b), finer silty-clayey sediments are characterized by the decrease of total sediment D50 values (~30 µm before 140 cm and 18 µm after this limit).

4.2. Palynological results of core MD08-3204 CQ

The description of palynological results led to the examination of four main palynozones (MD1 to MD4; Figs. 4 and 5). These zones were established based on pollen and dinocyst observations in terms of both concentrations (Fig. 4) and percentages (Fig. 5), coupled with a clustering analysis. The palynological data are not described and interpreted in the 196–134 cm interval (grey bands in Figs. 4 and 5) owing to potential taphonomic bias and possible remobilization (subsection 4.1.1.). The palynological data acquired in the 299–210 cm interval are not discussed from a stratigraphic point of view because of extremely high sedimentation rates**.** Moreover, this interval is marked by extremely low dinocyst concentrations (less than 50 dinocysts counted per level in the 299–210 interval; Figs. 4a, f). For these reasons, the palynological data have been summed to get an average picture of the interval in the discussion hereafter. Owing to the constant sedimentation rates, the palynological (pollen and dinocysts) signal is analyzed at a 100-year time resolution from 140 cm onward.

4.2.1. Diversity and concentrations

A total of 31 different dinocyst taxa were recognized in the whole core, with a mean taxon richness of 14 dinocyst taxa per slide, with lower diversity before 134 cm (i.e., 5.7 ka BP) and higher diversity after this limit (Fig. 4c; and related higher Margalef diversity in Fig. 4b). Total dinocyst concentrations (Fig. 4a) range between ~300 and 53,000 cysts/cm^3, with very low values estimated in the 290–196 cm interval (mean of 1,400 cysts/cm^3; MD1 excluding the 196–134 cm section). Higher concentrations are recorded in the upper part of the core, divided into three palynozones according to the main fluctuations of concentration values: MD2 (134–112 cm; 5.7–4.9 ka BP; mean of 4,600 cysts/cm^3), MD3 (112–49 cm; 4.9–2.4 ka BP; mean of 26,100 cysts/cm^3) and MD4 (from 49 cm or 2.4 ka BP; mean of 9,200 cysts/cm^3; Fig. 4a). Total

dinocyst concentrations (Fig. 4a; as well as the dominance index in Fig. 4d) are mainly influenced by *Lingulodinium machaerophorum* occurrences (Figs. 4a, e). Maximal dinocyst concentrations are therefore reached in zone MD3 (mean of 26,000 cysts/cm^3), in parallel with maximal percentages of *L. machaerophorum* at ~96% (Fig. 4e). Due to the low dinocyst counts (far below 100 specimens/slide) reached in zone MD1 (Fig. 4f: mean of 28 dinocyst counts per slide for the 7 samples between 290–196 cm), the dinocyst data obtained across this 200 yr-long interval (8.5–8.3 ka BP) were summed (194 dinocysts) providing mean dinocyst percentages for this interval (Fig. 5a and the following description of results).

Regarding pollen analyses, 95 different taxa were recognized in total with an average of 25 pollen taxa per slide, with lower diversity before limit a (134 cm) and higher diversity after this boundary (Fig. 4i; and related higher Margalef diversity in Fig. 4h). The maximal pollen diversity is recorded in zone MD4 (~26 different taxa per slide; Figs. 4h, i). Total pollen concentrations (Fig. 4g) range between ~2,700 and 38,000 grains/cm^3, with high values reconstructed in zone MD1 (mean of 20,299 grains/cm^3), and especially during the interval of finer sediments (mean of 29,500 grains/cm^3) that are favorable to a higher concentration of palynomorphs. Considering the upper part of the core, after 134 cm (i.e., 5.7 ka BP), higher pollen concentrations are recorded in zone MD3 (112–49 cm; 4.9–2.4 ka BP; mean of 11,900 grains/cm^3), while MD2 (132–112 cm; 5.7–4.9 ka BP; mean of 8,000 grains/cm^3) and MD4 (from 49 cm or 2.4 ka BP; mean of 5,700 grains/cm^3; Fig. 4g) are characterized by lower values. The pollen dominance index (Fig. 4j) is mainly determined by *Quercus* percentages (Fig. 4k) all along the core; the lowest values of this taxon being recorded in zone MD4, which is also characterized by the highest pollen diversity.

4.2.2. Description of palynological assemblages

Zone MD1 is characterized by the dominance of inner neritic (~62%; i.e., *Spiniferites lazus*, *Spiniferites bentorii*) and outer neritic (~24%; i.e., *Operculodinium centrocarpum* sensu *Wall & Dale, 1966*, *Spiniferites mirabilis*) taxa (Fig. 5a). Above 134 cm, zone MD2 corresponds to increasing percentages of *L. machaerophorum* (mean of 77%) and the decrease of other dinocyst taxa (Fig. 5a). In zone MD3, *L. machaerophorum* reaches maximum values above 80%, with two subzones that can be identified. In subzone MD3a, *L. machaerophorum* reaches its highest values in the whole study sequence (up to 95%), whereas subzone MD3b (80–49 cm) is characterized by the progressive rise of inner neritic taxa, mainly due to increasing percentages of *S. bentorii* and *S. lazus*. Finally, zone MD4 (49 cm onward; from 2.4 ka BP) is marked by a decrease of *L. machaerophorum* percentages (mean of 74%), as well as an increase of *Spiniferites* taxa and coastal heterotrophic percentages (Fig. 5a), especially in subzone MD4b (i.e., from 30 cm).

Regarding pollen assemblages (Fig. 5b), zone MD1 is characterized by occurrences of Amaranthaceae (mean of 12%), and high percentages of arboreal taxa (average of 77%), mainly represented by *Quercus* and *Corylus*. Zone MD2 is marked by lower percentages of Amaranthaceae and increasing values of riparian tree taxa, mainly due to the gradual rise of *Alnus* (Fig. 5b). Zone MD3 is characterized by the highest values of riparian taxa (21%), while thermophilic trees *Ulmus* and *Tilia* progressively decline. In subzone MD3b, the decrease in arboreal taxa (i.e., *Quercus* and *Corylus)* and the increase in Poaceae percentages are particularly obvious. In addition, occurrences of *Fagus* are noted. In zone MD3b, the decline of the forest system is associated with the increase of ruderal and adventitious taxa and is amplified in zone MD4 (Fig. 5b). The latter zone is characterized by the rise of Poaceae and a sharp decrease in arboreal taxa percentages. Sub-palynozone MD4b stands out by the highest occurrences of cultivated taxa (4%).

5. Discussion

5.1. Sedimentary evolution of the Armorican shelf over the last 10 kyrs BP

5.1.1. Sedimentation rates during the Holocene transgression

In the high sedimentation rate interval (~10–8.4 ka BP), higher sedimentation rates are recorded in the BQ (~4.5 mm/yr; Fig. 3a) compared to the northern GV (~0.66 mm/yr; Fig. 3b). This can be explained by the proximity to the coast of core MD08-3204 CQ (~7 km from present day coastline) and the shallowest depositional environment (~17 m deep today), whereas core VK03-58bis lies farther (~22 km from present day coastline) and deeper (~96 m deep today). Moreover, fine to medium sand sediments are found in core MD08-3204 CQ, reflecting more energetic marine conditions during the flooding of the BQ, whereas at that time the GV was already located in an open oceanic area.

Similar trends in sedimentation rates, occurring in the same temporal windows in both study cores, reflect a shared sedimentary evolution related to the evolution of the RSL rise through time (see Fig. 3 with the southern Brittany RSL rise from *García-Artola et al., 2018*). Specifically, both age-depth plots (Fig. 3) evidence a period of high sedimentation rates i) in the 8.5–8.3 ka BP interval for core MD08-3204 CQ (~4.5 mm/yr) and ii) in the 10–8.3 ka BP interval for core VK03-58bis (~0.6 mm/yr). The fast rhythm of the transgression (~10 mm/yr) during the final step of the rapid RSL rise (*García-Artola et al., 2018*) led to high sedimentation rates associated with the establishment of the Transgressive System Tract (TST; Figs. 3 and 6). At that time, the occurrences of inner and outer neritic dinocyst taxa together with Amaranthaceae pollen (Figs. 5 and 6) testify that the BQ is a subtidal bay close to extended maritime marshes and detrital sources also explaining extremely high continental palynomorph fluxes to the BQ (Fig. 6). The TST establishment is also recorded in the Loire estuarine system

(*Delaine et al., 2015*; *Arthuis et al., 2015*; *Arthuis, 2020*) that extended in the Gulf of Morbihan from ~9 to 5.8–5 ka BP (*Perez-Belmonte, 2008*).

Subsequently, and until 5.7 ka BP, a drop in sedimentation rates is recorded in both studied cores (0.24 and 0.01 mm/yr for cores MD08-3204 CQ and VK03-58bis, respectively; Fig. 3) synchronously with the slowdown of the RSL rise rates, as regionally recorded at ~6 ka BP (*Goslin et al., 2015*; *Stéphan et al., 2015*; *García-Artola et al., 2018*). The Maximum Flooding Surface (MFS) marks the end of the general transgression, inducing a reduction of the accommodation space and leading to lower sediment deposition. For the MD08-3204 CQ core, the interval of slowing RSL rise and decreasing sedimentation rates is associated with a reversed date suggesting a period of remobilization. Thus, we suggest a revision for the BQ model established by *Baltzer et al. (2014)* that previously discussed the establishment of the MFS at ~5 ka BP (Fig. 3a). According to our new chronostratigraphy and the consistent signal obtained with the GV, the transgressive deposit (i.e. TST) ends at 8.3 ka BP, and is followed by a period of sediment remobilization (i.e., MSF establishment) until 5.7 ka BP.

Then, from 5.7 ka BP, a resumption of sedimentation, at lower rates (~0.24 mm/yr and 0.22 mm/yr for cores MD08-3204 CQ and VK03-58bis, respectively) than during the pre-8.3 ka BP interval, occurs in a period of slower RSL rise (i.e., less than 1 mm/yr after 6 ka BP; *García-Artola et al., 2018*; Fig. 3) corresponding to the establishment of the Highstand System Tract (HST; Figs. 3 and 6). The increase of the continental-fluvial influence is observed over the Armorican shelf through higher percentages (Figs. 5a and 6) and fluxes (Fig. 6) of *L. machaerophorum*, almost monospecific today in estuarine sediments (*Morzadec-Kerfourn, 1976, 1977*; *Ganne et al., 2016*; *Lambert et al., 2017*), and of riparian pollen taxa (Fig. 5b), as recently discussed on the Armorican mid-shelf (*Penaud et al., 2020*). At the same time, high erosional episodes identified in the Gulf of Morbihan, and the Loire estuary, testify to a

predominant runoff and fluvial discharge to the Bay of Biscay (*Perez-Belmonte, 2008*; *Delaine et al., 2015*; *Arthuis et al., 2015*; *Arthuis, 2020*).

5.1.2. "The Turritella layer": a bio-stratigraphical indicator of the Maximum Flooding Surface establishment

The VK03-58bis core is characterized by a layer showing a high concentration of *Turritella communis* shells (Fig. 3b) and described as the "*Turritella* layer" (TL; *Bourillet et al., 2005*; *Naughton et al., 2007*; *Baltzer et al., 2015*). In this core, two shells dated at the base (160 cm: 8.4 ka BP) and at the top (149 cm: 7.5 ka BP) of the TL provide a minimal age extension of 900 years for this ~12 cm-thick deposit.

Previous studies suggested drastic environmental changes as potential drivers of the TL ending. First, a potential link between the TL and the abrupt North Atlantic climate shift of the 8.2 ka BP event was proposed (*Naughton et al., 2007*; *Baltzer et al., 2015*). It was then hypothesized that the North Atlantic sea-surface cooling and related decreasing salinity (*Alley et al., 2003*) could have explained the monospecific development of *T. communis* since these taxa are not sensitive to variations of these hydrological parameters (*Funder et al., 2002*; *Baltzer et al., 2015)*. The end of the TL was also attributed to a mortality event induced by the opening of the English Channel, then contributing to major hydrological and sedimentological changes in the north-eastern temperate Atlantic Ocean (*Naughton et al., 2007*). Finally, *Baltzer et al. (2015)* suggested that the abrupt sediment supply associated with the rapid RSL rise, and the related lack of oxygen for benthic organisms, could have been responsible for the *T. communis* death and burial of their shells.

The new AMS-^{14}C dates obtained for core VK03-58bis (Table 2) suggest that the TL is related to extremely low sedimentation rates (~0.01 mm/yr; Fig. 3b) at the end of the TST in the

Armorican shelf. In the TL, juvenile and adult specimens are found in a perfect taphonomic state owing to the absence of broken shells or abrasion marks (*Folliot, 2004*; *Baltzer et al. 2015*). This likely excludes strong bottom energetic currents during the TL interval and suggests an autochthonous origin and an "*in-situ*" preservation of *T. communis* shells in generally living position. A winnowing of fine particles (i.e., no observed sandy inputs or specific grain size distribution) by weak bottom currents may however have occurred, considering the present-day mud-burrowing mode of life of these filter-feeder gastropods (*Yonge 1946*; *Carter, 2008*). Both taphonomic considerations and ^{14}C-AMS dates therefore argue for a monospecific within-habitat preservation where fossil assemblages are time-averaged (*Walker and Bambach, 1971*; *Kidwell, 1997*; *Fujiwara et al., 2004*), thus implying a succession of several *T. communis* generations during a long-lasting period (i.e., here ranging between ~1 kyr minimum and 2.1 kyrs maximum) of low sediment supply. We therefore suggest that the TL represents a condensed level, occurring synchronously with the slower RSL rise rates at the end of the TST. According to this interpretation, the TL appears as a marker of the MFS in Holocene transgressive deposits of the Armorican shelf.

5.2. Palynological records along a proximal-distal gradient during the TST interval (8.5–8.3 ka BP)

In the lower part of core MD08-3204 CQ, between 290–196 cm (200 yrs: 8.5–8.3 ka BP), palynological results (dinocyst and pollen assemblages) were averaged (Fig. 5). In strictly the same Early Holocene interval, these new palynological data emanating from the inner shelf (i.e., 0–50 m deep) were compared with previously published data acquired from proximal coastal to distal marine domains along the Armorican shelf.

For this purpose, three cores were selected (Fig. 1a): i) the inner-shelf VC2012-08-PQP core (PROTEUS-DUNES cruises; *Shom, 2012*) hereafter referred to as core VC-08, retrieved at 28

m depth in the shallow coastal Bay of Douarnenez (BD; 17 points extracted from *Lambert et al., 2019*), ii) the mid-shelf VK03-58bis core (Vibarmor cruise; *Le Roy et al., 2003*), retrieved at 96 m depth in the South Glénan sector of the Grande Vasière (GV; 5 points extracted from *Naughton et al., 2007* for pollen and *Penaud, pers. comm.* for dinocyst assemblages), and iii) the distal marine MD95-2002 core (IMAGES 101 expedition; *Bassinot and Labeyrie., 1996*), retrieved at 2,174 m depth on the Meriadzek Terrace (3 points extracted from *Zumaque et al., 2017* for dinocyst and *Fersi et al., in prep.* for pollen assemblages).

5.2.1. Averaged 8.5–8.3 ka BP dinocyst observations

From inshore to offshore environments, among a palynomorph sum including pollen grains, spores, and dinocysts, the dinocyst proportion increases from < 10% in the bays (cores MD08-3204 CQ and VC-08) to slightly over 50% in the mid-shelf (core VK03-58bis) and offshore (core MD95-2002) (Fig. 7a). The proximity to the close terrestrial domains, and hence to the pollinic production sources, appears responsible for the high pollen grain percentages recorded in the bays (Fig. 7a). A maximum dinocyst diversity is recorded in core VK03-58bis (Fig. 7b), mainly subjected to oceanic influences at that time (*Penaud et al., 2020*). Dinocyst assemblages in the two shallowest cores are dominated by inner neritic taxa (i.e., especially *S. bentorii*, accompanied by *Spiniferites membranaceus- Spiniferites belerius, Spiniferites delicatus,* and *S. lazus*) that represent a minor part of the assemblage in the mid-shelf and barely occur offshore (Fig. 7b). Considering the shallow Quiberon and Douarnenez bays, dinocyst assemblages are consistent with sedimentological studies describing fluvial environments subject to tidal influences (*Jouet et al., 2003*; *Le Roy and Jouet, 2005*; *Baltzer et al., 2014*; *Gregoire et al., 2017*; *Lambert et al., 2019*). A slight difference is seen among inner neritic assemblages with major occurrences of *S. bentorii* and cysts of *Pentapharsodinium dalei* in the more enclosed BD, replaced by *S. lazus* and by the apparition of the neritic group, *Spiniferites ramosus-*

Spiniferites bulloideus, in the BQ. These assemblages reach their highest values in core VK03-58bis (Fig. 7b), testifying to their association with peri-Brittany shelf waters (*Morzadec-Kerfourn, 1977*; *Penaud et al., 2020*; *Lambert et al., 2022*). In more distal environments, dinocyst assemblages are mainly composed of outer neritic taxa, especially *S. mirabilis* and *O. centrocarpum*, worthy of note are the unique occurrences of full-oceanic *Impagidinium* species and the absence of the estuarine *L. machaerophorum* taxon in core MD95-2002 (Fig. 7b). A steeper marine influence is thus recorded in the distal cores during the Early Holocene, as recorded during the Mid to Late Holocene (*Penaud et al., 2020*) and in present-day (*Lambert et al., 2022*) dinocyst assemblages along the same inshore-offshore transects.

5.2.2. Averaged 8.5–8.3 ka BP pollen observations

During the 8.5–8.3 ka BP interval, a short temporal window during the wider Mesolithic cultural period (i.e., 10–7 ka BP; 8.5–5.1 ka BC in western Brittany), anthropogenic changes appear limited, as testified by high arboreal taxa percentages (i.e., 80 to 90% in coastal to mid-shelf cores) and very low values of anthropogenic taxa (i.e., not exceeding 1%; Fig. 8a). The high representation of arboreal taxa, related to a still large forest cover on the continent, may additionally be explained by the pollination period, especially that of *Quercus* whose pollen grains are present in the atmosphere mainly during spring months (March to June; *Rodríguez-Rajo et al., 2005*; *García-Mozo et al., 2006*). In a high boreal summer insolation context, *Penaud et al. (2020)* suggest that the high pollination of trees, coupled with spring to summer rainfall regimes and related fluvial discharge, could amplify the signature of *Quercus* pollen grains in the platform, therefore accounting for the highest arboreal pollen fluxes recorded in the Armorican shelf during the Early Holocene.

549 The more distal marine sequence (i.e., core MD95-2002) is characterized by the highest pollen
550 diversity and the highest herbaceous percentages when compare with the inshore-offshore
551 transect (Fig. 8a). The most diverse pollen signature of core MD95-2002 (*Fersi et al., in prep*)
552 may be explained by the multi-catchment area pollen sources (i.e., macro-regional fluvial
553 signatures coming from Loire, Gironde, South Brittany, and English Channel watersheds). In
554 contrast, the two bays imply pollen sources from more limited catchment areas close to the
555 collected cores (i.e., MD08-3204 CQ at ~5 m depth and VC-08 at ~16 m depth, under a water
556 column that was 12 m below the present-day sea level; *García-Artola et al., 2018*).
557 Furthermore, core MD92-2002 presents a unique Cupressaceae signature (including *Juniperus*),
558 combined with boreal forest taxa (i.e., *Picea-Abies*) and high percentages of the pioneer taxon
559 *Betula* (Fig 8b), which are likely associated with a northern European continental signature
560 transported by the English Channel (*Fersi et al., in prep*). In addition, Mediterranean trees
561 (grouping *Quercus ilex* and *Quercus suber*) are recorded at ~1-2%, in the deep core, but also in
562 the mid-shelf sequence (i.e., core VK03-58bis; Figs. 8b, c), and may correspond to southern
563 French river watersheds, implying mainly Loire and to a lesser extent Gironde river influences
564 (*Penaud et al., 2020*).

565 The pre-6 ka BP interval, still characterized by high RSL rise rates (*García-Artola et al., 2018*)
566 and the intense activity of the North Atlantic Current (*Ayache et al., 2018*), was described as a
567 "summer-prevailing mode" in the southern Brittany platform (*Penaud et al., 2020*), i.e., as a
568 prevalent NW to SE shelf residual circulation in the Bay of Biscay. This prevalent oceanic
569 influence over the platform may explain the high dinocyst diversity recorded in the mid-shelf
570 (Fig. 7b). However, the occurrences of Mediterranean tree pollen in the two more distal cores
571 attest to common continental sources inherited from southern France catchments (Figs. 8b, c).
572 In the deep MD95-2002 core, the unique occurrences of *Impagidinium* spp.,
573 *Nematosphaeropsis labyrinthus*, *Brigantedinium* spp. oceanic taxa (Fig. 7b), and Cupressaceae

and *Picea-Abies* pollen grains (Figs. 8b, c), indicating rather a distant northern European continental source carried by oceanic currents that however barely affect the mid-shelf. We hypothesize that a hydrological front, formed in the northern Bay of Biscay during summer months, may have prevented the summer transportation of these northern continental sources to the mid-shelf, while a break of the thermohaline front during winter months may have favored the transport of southern continental sources up to the northern Bay of Biscay. This would correspond to the opposite configuration to the one prevailing for the present-day seasonal hydrological mechanism operating in the Bay of Biscay (i.e., "winter prevailing mode", see Fig. 1a), characterized today by the establishment of the thermohaline front during winter months (*Castaing et al., 1999*; *Costoya et al., 2016*) and since ~3.3 ka BP (*Mojtahid et al., 2019*; *Penaud et al., 2020*).

5.2.3. *Quercus vs. Corylus signature in space and time*

Arboreal taxa are dominant along the inshore-offshore transect (Fig. 8a) as commonly observed and thoroughly discussed in sediment archives (*Broström et al., 2008*; *Mazier et al., 2008, 2015*; *Lebreton et al., 2010*; *Sjögren et al., 2015).* In addition, the anemophilous *Pinus* pollen grains are over-represented in marine sequences (Fig. 8b) due to their strong capacity of dispersion (*Turon, 1984*; *Holmes, 1994)*. Excluding *Pinus* and *Picea-Abies* taxa from the arboreal sum (Fig. 8c), deciduous *Quercus* pollen grain percentages increase from the bays (~same values for both shallow environments) to the mid-shelf, while those of *Corylus* decrease along this same gradient. Among the two other temperate forest taxa found in the northern European sediment archives, we suggest that the *Corylus* signal may decrease with the distance from the coast, boosting the deciduous *Quercus* expression in more distal sediments (Fig. 8c). This may explain the fact that the *Corylus* percentages are always higher than the *Quercus* ones, regardless of the period considered over the last 7 kyrs, in south-western Brittany peat deposits

(*Fernane et al., 2014*), whereas the opposite is observed in the southern Brittany coastal (*Fernane et al., 2015)* and mid-shelf (this study; *Penaud et al., 2020*) environments. In addition, it should be pointed out that *Quercus* has a high degree of resistance to oxidation (*Lebreton and al., 2010*) that may partly explain its over-representation in marine environments.

Moreover, previous studies of the Mid to Late Holocene showed an anti-correlation between deciduous *Quercus* and *Corylus* pollen percentages, with *Quercus* contractions and *Corylus* expansions, and *vice-versa*, at a pluri-decadal timescale (*Joly et Visset, 2009*; *Fernane et al., 2014*). Knowing that *Corylus* pollination takes place during winter months (January to March; *Bégeot, 1998*; *Olsen et al., 2000*), contrary to deciduous *Quercus* pollination that occurs during spring months (March to June; *Rodriguez-Rajo et al., 2005*; *García-Mozo et al., 2006*), *Corylus*/*Quercus* anticorrelations at an infra-orbital timescale could be explained by a stronger fluvial influence due to enhanced precipitation fostering the *Corylus* signature during the winter season. In north-western Europe, *Alnus* flowering is very close to that of *Corylus* (*Puc and Kasprzyk, 2013*). A correlation between *Alnus*, and also *Corylus*, and intensified fluvial discharge is identified in modern sediments from the Bay of Brest (*Lambert et al., 2017*). For this reason, both *Alnus* and *Corylus* allowed understanding intensified winter paleo-discharge in the Bay of Brest over the last 2.5 kyrs BP (*Lambert et al., 2020*). In addition, *Penaud et al. (2020)* used the *Corylus*/*Quercus* ratio over the last 7 kyrs BP (core CBT-CS11 in the southern Brittany shelf; Fig. 1b) and demonstrated its common trend with alluvial taxa (especially *Alnus*). From this perspective, *Corylus* (and *Alnus*) vs. *Quercus* pollen percentage fluctuations detected at a pluri-decadal timescale in Holocene records, may be partly reconciled by considering periods of enhanced winter precipitation and related fluvial discharge when *Corylus* percentages increase, and vice versa.

5.3. Natural vs. anthropogenic impacts since 5.7 ka BP along an inshore-offshore gradient at the scale of the South Brittany platform

After 5.7 ka BP, in the MD08-3204 CQ core, the resumption of mixed estuarine-marine sedimentation leads to a continuous palynological record in the BQ. In order to better understand the paleoenvironmental changes that occurred along the South Brittany coast over the last 5.7 kyrs BP (at ~100 yrs time resolution), the main palynological results acquired in this study were selected (i.e., *L. machaerophorum, Alnus, Corylus, Quercus,* Poaceae and API; orange curves in Figs. 9 and 10). These data are discussed in parallel with two sedimentological records covering the last 7 kyrs BP (Fig. 2b). First, the mid-shelf CBT-CS11 core (Figs. 1a, b; CABTEX cruise; *Dussud, 2010*) was acquired at 73 m depth in the south-Penmarc'h sector of the GV (*Penaud et al., 2020*: ~80 yrs time resolution between 7–0.5 ka BP; blue curves in Figs. 9 and 10). Secondly, the continental GL3 core (*Fernane, 2014*) was retrieved in the South Brittany coastal wetland of Guidel (Figs. 1a, b) and corresponds to an ancient ria progressively transformed into a maritime coastal marsh during the Holocene transgression (*Fernane et al., 2015*: ~85 yrs time resolution between 7–0.6 ka BP; green curves in Figs. 9 and 10).

5.3.1. Fluvial hydrosystem processes and related shelf sedimentation

Dinocyst data acquired in the BQ over the last 5.7 kyrs BP show a clear dominance of *L. machaerophorum*, that started to increase at ~5.9 ka BP according to the 7 kyr-long CBT-CS11 core (*Penaud et al., 2020*; Fig. 9). This species is tolerant to large drops in salinity and is well known to proliferate in brackish environments (*Reid, 1975*; *Morzadec-Kerfourn, 1977, 1992, 1997*). At the same time, pollen grains of the riparian taxon *Alnus*, a hydrophilous tree developing mainly along freshwater bodies, reaches its maximum values in both MD08-3204 CQ and CBT-CS11 cores (Fig. 9). The 5.7 ka BP limit corresponds to the major inflection in

the RSL rise rates occurring at ~6 ka BP (*Goslin et al., 2015*; *Stéphan et al., 2015*; *García-Artola et al., 2018*), then corresponding to the stabilization of fluvial systems (*Penaud et al., 2020*). The riparian vegetation (i.e., *Alnus*) then progressively colonizes coastal marshes, which in turn promotes the fixation of vegetation in riverbanks and valley alluviation (*Penaud et al. 2020*). The increase in estuarine-sensitive taxa (i.e., *Alnus* and *L. machaerophorum*; Fig. 9) in coastal areas argues for a stronger fluvial influence on the shelf since 5.7 ka BP, which is consistent with the HST establishment (subsection 5.1.1). The typical neritic dinocyst assemblage, obvious during the TST configuration, appears extremely different when considering dinocyst percentages after 5.7 ka BP that are characterized by the over-representation of *L. machaerophorum* (mean of 83%; Fig. 6). However, if *L. machaerophorum* is excluded from the main sum, dinocyst percentages appear quite similar to the pre-5.7 ka BP period (Fig. 6). This argues for an allochthonous signal of the estuarine-sensitive taxon *L. machaerophorum*, likely carried to the Armorican shelf by main river discharge, especially the Loire and Vilaine rivers (Fig. 6). Furthermore, *Delaine et al. (2015)* examined the Holocene sediment infilling of the upstream Loire Valley and recorded a high erosional regime of the Loire system between ~5.8–2.1 ka BP in a context when sedimentation rates exceeded the RSL rise rates. This may have led to a shift of the sediment depo-center towards the Armorican shelf, as testified by the coarser sedimentation recorded in core CBT-CS11 up to ~3.3 ka BP (*Mojtahid et al., 2019*; *Penaud et al.., 2020*; D50 $CaCO_3$ free in Fig. 9). After 3.3 ka BP, the decrease of estuarine-sensitive taxa (i.e., *Alnus*, *Corylus* and *L. machaerophorum*) percentages and sediment grain-size values recorded in core CBT-CS11 (Fig. 9) suggest a decreasing influence of the paleo-Loire erosional dynamics. Geomorphological studies have shown that the sediment load may have exceeded the transport capacity leading to a Loire riverbed elevation at ~2.7 ka BP (*Castanet, 2008*; *Arthuis, 2020*). The progressive infilling of the

estuarine system contributed to the decrease of the river slope and likely also the load-transport capacity of the Loire river at ~3 ka BP.

In contrast, in core MD08-3204 CQ, estuarine-sensitive taxa percentages remain quite constant around 3 ka BP (Fig. 9). This may be explained by the location of the BQ, semi-isolated by the Quiberon peninsula and islands (*Houat*, *Hoedic* and *Belle-Ile*; Fig. 1b), then exposed to the additional influences of the Gulf of Morbihan and Bay of Vilaine fluvial sediment supply (*Menier et al., 2010, 2014*). At that time, the Vilaine river dynamics (different from the Loire river ones) may have maintained the sediment load to the platform in the BQ. It is worth noting that the Vilaine fluvial system has now been totally altered since the construction of the Arzal dam in 1970, reducing water fluxes (~71 m^3/s between 1970 and 2000 in Rieux, *www.hydro.eaufrance.fr*) and thus sediment transfers to the platform, which are therefore no longer comparable today to the above-described Late Holocene discussion for the BQ. After 2.4 ka BP, the decline of the general forest cover (i.e., *Alnus*, *Quercus*, *Corylus*; Fig. 9) is accompanied by an increase in Poaceae and Anthropogenic Pollen Indicators (API; Figs. 9 and 10), testifying to the continentalization of the coastal environment under the strong human-forced influence on freshwater bodies (*Delaine et al., 2015*).

5.3.2. The anthropogenic pollen signature along the South Brittany coast

The continental core GL3 (*Fernane et al., 2015*) provides a local anthropogenic signal restricted to southern Brittany watersheds, whereas the two shelf cores CBT-CS11 (*Penaud et al., 2020*) and MD08-3204 CQ (this study) provide a more regional averaged anthropogenic signal at the scale of western French watersheds involving Loire, Vilaine and southern Brittany rivers (Fig. 1b).

In our study, during the Neolithic interval (7–4.2 ka BP / 5–2.2 ka BC), arboreal taxa percentages (especially *Quercus*) remain high in the two shelf sequences, whereas in the continental site of Guidel, sharp fluctuations affect the arboreal trend (i.e., *Quercus* and *Corylus*) and are explained mainly by recurrent increases in Poaceae percentages (Fig. 9). In this site, the anthropogenic activity is confirmed by co-occurrences of ruderal and adventitious taxa and discrete occurrences of cultivated plants, occurring mainly in the 6.4–5.1 ka BP interval (/4.4–3.1 ka BC; Fig. 10c; *Fernane et al., 2015*). Along the South Brittany coast, several continental palynological studies (*Visset et al., 1996*; *Gaudin, 2004*; *Visset and Bernard, 2006*) attest to Neolithic agro-pastoral activities with sporadic *Cerealia*-type occurrences. On land, the anthropogenic signal is captured by small sedimentary basins, such as the coastal wetland of Guidel. Although deforestation and agro-pastoral practices are well-referenced on land, ruderal and adventitious taxa remain low in shelf cores with no co-occurrences of cultivated taxa (Figs. 10a, b). We suggest that during the Mid-Holocene, Poaceae and API, already weakly recorded far from emission sources, are insufficiently transmitted to the platform to be significantly recorded in marine sediments.

From 4.2 ka BP (i.e., the start of the Late Holocene from a stratigraphical point of view; *Walker et al., 2019*), a major reorganization affects oceanic and atmospheric dynamics, as recently discussed at the Bay of Biscay scale (*Penaud et al., 2020*). The winter insolation at 65°N increases along the Holocene favoring wetter and milder winters over northern Europe (*Benito et al., 2015*). The intensification of a winter precipitation regime led to enhanced river discharge, as shown by the high percentages (Figs. 5a and 6) and fluxes (Fig. 6) of *L. machaerophorum*. Subsequently, higher river discharge led to the establishment of the winter thermohaline front at ~3.3 ka BP along the BoB (*Mojtahid et al., 2019*; *Penaud et al., 2020*). This configuration enhanced the transmission of the API signature from the watersheds to coastal waters. From 4.2 ka BP (/2.2 ka BC), and across the Bronze and Iron Ages (4.2–2 ka

BP / 2.2 ka BP–50 BC), all sequences point to a synchronous arboreal percentage decrease, together with the progressive increase in Poaceae percentages (Fig. 9). From this boundary, the two shelf sequences show an apparent discontinuous record related to the rise of API percentages (i.e., adventitious, ruderal and cultivated taxa; Figs. 10a, b), whereas the rise in API percentages is continuous from 3.3 ka BP at Guidel (Fig. 10c). This palynological trend confirms the major human-induced landscape transformation that occurred under enhanced agro-pastoral activities discussed with archeological (*Pailler and Nicolas, 2019*) and continental palynological (*Marguerie, 1990, 1992, 1993*; *Gaudin, 2004*; *van Beek et al., 2018*) data. In Guidel, a second major shift in terms of human impact, highlighted by the sharp drop of arboreal taxa and the related increase of Poaceae percentages (Fig. 9), occurs at around 2.4 ka BP (/450 BC), i.e., at the second Iron Age. In all sequences, the API signature tends to increase at ~1.2 ka BP (Fig. 10). At that time, the maximum percentages of cultivated taxa are due to the intensification and diversification of agriculture practices in western France (*Marguerie, 1992*; *Visset et al., 1995*; *Gaudin, 2004*; *Fernane et al., 2015*), showing the massive opening of the landscape and foreshadowing the present-day bocage organization of the area (*Barbier, 1999*; *Cyprien, 2002*; *Marguerie, 2003*).

5.3.3. Impact of multi-secular hydro-climatic forcing on the Anthropogenic Pollen Indicator (API) record

Guidel (continental, core GL3) and Quiberon (protected shelf, core MD08-3204 CQ) environmental contexts are mainly associated with South Brittany watersheds (Fig. 1b). Furthermore, cores MD08-3204 CQ and CBT-CS11 (Fig. 1b) are exposed to additional input from the Loire River especially since the stabilization of the sea level at ~6 ka BP and the subsequent increase of winter fluvial discharge at 4.2. ka BP (subsection 5.3.1.). It is thus possible to compare and discuss these three cores as end-members in terms of continental

744 sources with South Brittany proximal inputs (i.e., Laïta River influence; Fig. 1a) for core GL3,
745 Loire River for core CBT-CS11, and mixed river sources for core MD08-3204 CQ.

746 In core GL3, the increase in API percentages is obvious across the intervals 6.4–5.1, 3.3–2.7
747 and 1.6–1.2 ka BP (grey bands in Fig. 10), identified in *Penaud et al. (2020)* as periods
748 characterized by enhanced subpolar gyre (SPG) strength at times of Bond events 4, 2 and 1,
749 respectively (*Bond et al., 1997, 2001*). These API increases are also observed in core MD08-
750 3204 CQ, except for the 6.4–5.1 ka BP interval that corresponds to a Mid-Holocene period
751 when we argue for a less continental influence and therefore a lower API transmission to the
752 platform (subsection 5.3.2.). General intensification of anthropogenic activities during these
753 three intervals was not recorded in previous continental studies (*Visset et al., 1995, 1996*;
754 *Gaudin, 2004*; *Visset and Bernard, 2006*; *van Beek et al., 2018*). Regarding core CBT-CS11,
755 the API signal seems to show an opposite behavior, although the anthropogenic history of the
756 Loire watersheds is not opposite to that of the South Brittany ones. The palynological data
757 acquired on this mid-shelf core were previously discussed in the context of a millennial-scale
758 mechanism implying SPG strength coupled with natural atmospheric oscillations (*Penaud et*
759 *al., 2020*). In this model, North Atlantic gyre responses are supposed to be strongly related to
760 persistent North Atlantic Oscillations (NAO) configurations, even though a large non-linearity
761 exists today regarding gyre responses to the atmospheric forcing (*Lohmann et al., 2009*). Hence,
762 stronger Loire river discharge would represent a conjectural phenomenon of weakened SPG
763 influence under recurrent negative NAO-like modes (*Benito et al., 2015*). This would explain
764 a higher transmission of the API signal to the mid-shelf (core CBT-CS11) outside the Bond
765 events (higher API amplitudes in between the grey bands identified in Fig. 10a). This model
766 appears consistent with the stronger API detection observed in core GL3 (Fig. 10c) during
767 periods of enhanced SPG, in a general context of the northern location of the westerly storm
768 tracks (*Giraudeau et al., 2010*; *Goslin et al., 2018*; *Lambert et al., 2020*; *Penaud et al., 2020*)

with related increases of winter precipitation and fluvial discharge over northern Europe (*Hurrell, 1995*; *Hurrell et al., 2003*; *Tréguer et al., 2014*). Interestingly, it appears that the BQ could be compared to the observations made at Guidel, with however a less clear-cut API signature (Fig. 10b). From 5.7 ka BP, the BQ thus appears as a pivotal zone characterized by a stronger diversity of continental inputs related to different forcing also implying climate regimes at an infra-orbital timescale previously discussed and better expressed with core CBT-CS11.

Then, from 1.2 ka BP (/ 750 AD), in all cores the anthropogenic influence is characterized by highest amplitude peaks (Fig. 10). This boundary, corresponding to the start of the Middle Ages, appears as a limit from which anthropogenic forcing may outweigh the natural climate variability at the sub-orbital timescale.

6. Conclusion

Various factors forced coastal paleoenvironmental changes and palynological records during the Holocene, including the Relative Sea Level (RSL) rise that modified sedimentation processes, the fluvial discharge affected by both atmospheric and oceanic dynamics, and the anthropogenic impact. The present study examines Holocene paleoenvironmental changes along the Armorican shelg through a compilation of previously published and recently acquired data. First, new chronostratigraphies of the inner shelf MD08-3204 CQ (Bay of Quiberon, BQ) and mid-shelf VK03-58bis (Grande Vasière, GV) cores allowed refining the sedimentation model of the Armorican shelf. In addition, the new palynological (pollen and dinocyst) data acquired in core MD08-3204 CQ complete a set of pre-existing data acquired from the continental to the mid-shelf domains. This comparative approach has brought about a synthesis of the major environmental and hydrological reorganizations that affected the Armorican shelf over the last 10 kyrs BP:

- *From 10 to 8.3 ka BP*. The still strong Early Holocene RSL rise rates are responsible for the high sedimentation (~4.5 mm/yr in the BQ and ~0.66 mm/yr in the GV) rates leading to the Transgressive System Tract (TST) establishment over the Armorican shelf.
- *From 8.3 to 5.7 ka BP*. The slowdown of the RSL rise rates leads to a reduced accommodation space and to sedimentary remobilization in the BQ. In the GV, the condensed level corresponding to the already know "*Turritella* layer" is now identified between 8.4 and 6.3 ka BP, and appears as a biostratigraphical marker of the Maximum Flooding Surface (MFS) establishment in the Holocene sediments of the Armorican shelf.
- *From 5.7 to 3.3 ka BP*. The RSL slowdown and the reduced accommodation space, bringing low sedimentation rates (~0.24 mm/yr in the BQ and ~0.22 mm/yr in the

GV), led to the establishment of the Highstand System Tract (HST). As evidenced by the rise of estuarine-sensitive taxa (i.e., *Alnus* and *L. machaerophorum*), the fluvial influence, mainly from the Loire river whose load-transport capacity remains important, is growing on the platform.

- *From 3.3 to 2.4 ka BP*. The Loire River transport capacity declines, leading to a decrease in the erosive dynamics of the paleo-Loire. At that time, a different hydro-sedimentary dynamic of the Vilaine River likely maintained a high sediment load over the BQ.
- *Since 2.4 ka BP*. A continentalization of coastal ecosystems is widely recorded. Increases of both human activities and fluvial influences provide for a better transport of Anthropogenic Pollen Indicators (API), then better recorded over the platform, especially from 1.2 ka BP at the start of the Middle Ages.

By comparing multiple palynological sequences, located from onshore to offshore domains, our study also demonstrates the complexity of the API record during the Mid to Late Holocene. We suggest that the intensification of the fluvial discharge over the South Brittany watersheds during periods of subpolar gyre (SPG) strengthening tends to enhance continental palynomorph fluxes, particularly API, in Brittany coastal domains. Conversely, a weakened SPG associated with an intensified winter precipitation regimes over southern Loire catchments would tend to increase the API detection on the mid-shelf. In conclusion, at an infra-orbital timescale, the API signal detected in shelf sediments appears strongly connected to the hydro-climatic control on precipitation and related fluvial discharge. Without a fine understanding of all forcing parameters, discussing human dynamics from marine sediments would be biased by natural controls that deserve to be deconvoluted as a first step.

7. Acknowledgments

This work was part of a PhD thesis (Ophélie David) financed by the UBS (Univ. Bretagne Sud) and UBO (Univ Brest). We thank captains, crews, and scientific teams of the different cruises that collected both main study cores: the MD08-3204 CQ core (BISCOT campaign onboard the *Marion Dufresne*; MD169/MICROSYSTEMS cruise, 2008; IPEV) and the VK03-58bis core (Ifremer research project "*Défi Golfe de Gascogne*"; Vibarmor cruise, 2003 onboard the *Côtes de la Manche*). For the other cores discussed in the manuscript, we are indebted to the research projects involved in core retrieval and data acquisition (1) CBT-CS11 core (in *Penaud et al., 2020*): CABTEX cruise by the Ifremer onboard the R/V *Pourquoi Pas?* (*Dussud, 2010*); CNRS-INSU project HCOG2 (2013-2014) and ANR "HAMOC"; 2) VC2012-08-PQP core (in *Lambert et al., 2019*): PROTEUS-DUNES cruises; *Shom, 2012;* 3) GL3 core (*in Fernane et al., 2015*): ANR "COCORISCO", Brittany region project "PHILTRE"; 4) MD95-2002 core (in *Zumaque et al., 2017*): IMAGES 101 expedition; *Bassinot and Labeyrie (1996)*; ANR "HAMOC".

The palynological analysis of core VK03-58bis received fundings from a CNRS-INSU project HCOG2 (2013-2014) "*Forçages climatiques Holocène et répercussions Côtières et Océaniques dans le Golfe de Gascogne*" (coord. A. Penaud) as part of the LEFE-IMAGO research program. We thank Muriel Georget (EPOC; Univ. Bordeaux) and Pierre-Olivier Coste (Geo-Ocean, Univ. Brest) for their palynological laboratory assistance for the VK03-58bis and MD08-3204 CQ cores, respectively. To the QUIPALPLO project (coord. A. Baltzer), financed by OSUNA (Observatoire des Sciences de l'Univers de Nantes Atlantique), made possible some palynological analyses realized during the M2 internship of M. Herlédan (2019/2020). Some dates were obtained thanks to the French ARTEMIS ^{14}C-AMS platform, and the others were acquired at the Poznán Radiocarbon Laboratory and Beta Analytics. We are also grateful to Anne Véronique Walter-Simonnet (UMR 6249 Chrono-environnement; Univ. Bourgogne

Franche-Comté) who carried out the grain size, calcimetry, and TOC analyses of core MD08-3204 CQ. The authors are grateful to the ZABrI ("*Zone Atelier Brest Iroise"*, CNRS-INEE) and the ArMeRIE program funded by the UBO (Univ Brest) for fruitful interdisciplinary exchanges about human dynamics and Holocene paleoenvironments. This work was supported by the ISblue project (Interdisciplinary graduate school for the blue planet, ANR-17-EURE-0015), co-funded by a grant from the French government under the program "Investissements d'Avenir".

8. Data availability

All the data acquired on cores MD08-3204 CQ and VK03-58 bis, and discussed in the manuscript are available in the SEANOE repository: https://doi.org/10.17882/86430

9. Table captions

Table 1: MD08-3204 CQ AMS-^{14}C dates. In grey: dates previously published in *Baltzer et al. (2014)*. In black: new dates from this study acquired at the Poznań Radiocarbon Laboratory (Poz-x) and ARTEMIS (SacA x). All AMS-^{14}C dates were calibrated with the CALIB 7.1 software using the IntCal20 calibration curve (*Stuiver and Reimer, 1993*; *Reimer et al., 2020*), first considering a reservoir age of -400 ± 45 years to radiocarbon dates (point 1559 for the lower Loire in the marine20 database; *Tisnérat-Laborde et al., 2010*).

Code	Depth (cm)	Sample nature	Age ^{14}C BP ± error		Age min (mean) max Cal BP
Lyon 6307	20	*Turritella communis*	1510	30	955 **(1011)** 1067
Poz-113445	35	*Turritella communis*	2355	30	1820 **(1884)** 1948
Poz-33086	47	*Turritella communis*	2745	35	2312 **(2400.5)** 2489
Poz-113447	70.5	Bivalve	3585	30	3361 **(3407.5)** 3454
Poz-33089	79	*Turritella communis*	3850	40	3616 **(3724)** 3832
Poz-26298	93	*Turritella communis*	4190	35	4082 **(4187)** 4292
Poz-117547	111	Shell debris	4755	35	4847 **(4913.5)** 4980
Poz-113448	134	Gastropod	5420	35	5657 **(5776)** 5895
Poz-117549	152	Shell debris	5095	35	5320 **(5400)** 5480
Poz-117550	196	Bivalve	7960	40	8350 **(8375.5)** 8401
SacA 29329	225	Shell debris	8060	40	8386 **(8462.5)** 8539
SacA 29330	231	Shell debris	8160	45	8422 **(8511.5)** 8601
SacA 54334	235.5	Gastropod	8145	35	8442 **(8517)** 8592
SacA 32028	241.5	Gastropod	8025	30	8385 **(8403.5)** 8422
Poz-113449	287	Gastropod	8210	50	8429 **(8576.5)** 8724

Table 2: VK03-58bis AMS-^{14}C dates. In grey: dates previously published in Naughton *et al. (2007)*. In black: new dates from this study acquired at the Poznań Radiocarbon Laboratory (Poz-x), ARTEMIS (SacA x), and Beta Analytics (BETA-x). All AMS-^{14}C dates were calibrated with the CALIB 7.1 software using the IntCal20 calibration curve (*Stuiver and Reimer, 1993*; *Reimer et al., 2020*), first considering a reservoir age of -400 ± 45 years to radiocarbon dates (point 1559 for the lower Loire in the marine20 database; *Tisnérat-Laborde et al., 2010*).

Code	Depth (cm)	Sample nature	Age ^{14}C BP ± error		Age min (mean) max Cal BP
Poz-47041	32	Benthic foraminifera	2005	30	1408 (**1471.5**) 1535
Poz-47042	57	Benthic foraminifera	2810	70	2340 (**2526.5**) 2713
Poz-47043	92	Benthic foraminifera	3930	30	3714 (**3760**) 3806
Poz-10166	106	*Turritella communis*	3820	30	3572 (**3647.5**) 3723
SacA55613	110	*Turritella communis*	4110	30	3974 (**4038**) 4102
BETA-550086	125	Benthic foraminifera	5410	30	5653 (**5710**) 5767
Poz-47044	137	Benthic foraminifera	5940	40	6280 (**6341**) 6402
SacA55614	140	*Turritella communis*	7295	30	7678 (**7712.5**) 7747
Poz-10167	149	*Turritella communis*	7020	40	7431 (**7476.5**) 7522
Poz-10168	160	*Turritella communis*	8030	40	8369 (**8444.5**) 8520
Poz-10170	177	*Turritella communis*	8170	40	8429 (**8515.5**) 8602
BETA-550087	179	Benthic foraminifera	7900	30	8321 (**8347**) 8373
BETA-550088	210	Benthic foraminifera	8940	30	9486 (**9414.5**) 9543
Poz-10171	226	*Turritella communis*	8240	40	8521 (**8648**) 8775
BETA-550089	266	Benthic foraminifera	9400	40	10170 (**10201**) 10235

884 **Table 3:** This table gathers core MD08-3204 CQ data discussed in this study and describes the
885 methodology used to calculate palynological relative abundances, absolute concentrations, and
886 indexes, as well as dinocyst and pollen groups made according to ecological affinities (*Penaud*
887 *et al., 2020*).

888

MD08-3204 CQ data		METHODOLOGY
PALYNOLOGICAL REPRESENTATION	**Palynomorph relative abundances (%)**	Pollen percentages are calculated using a main sum excluding i) *Pinus* counts (*Pinus* pollen grains thus always tend to be over-represented in marine sediments due to better dispersal and conservation), ii) spores and iii) indeterminable pollen grains. Dinocyst percentages are calculated on a sum of total dinocysts excluding pre-Quaternary specimens.
	Palynomorph absolute concentrations (taxa/cm^3)	Palynomorph concentrations are based on the marker grain method with *Lycopodium* spores (de Vernal et al., 1999; Mertens et al., 2009); calibrated tablets of known numbers of spores (here 28 848) being added to each sample before chemical treatments.
	Diversity (Margalef) index	(S-1)/ln(n) where S is the number of taxa per sample and n is the number of individuals (pollen grains or dinocysts) counted in each sample.
	Dominance index	Dominance ranges from 0 (all taxa are equally present) to 1 (one taxa dominates the assemblage). Dominance=1-Simpson index.
	Taxon richness	Number of different taxa present in each analyzed level
DINOCYST GROUPS	**Sum inner neritic taxa (Cysts of phototrophs or mixotrophs)**	*Spiniferites bentorii* (Sben), *Spiniferites lazus* (Slaz), *Spiniferites membranaceus* (Smem), *Spiniferites belerius* (Sbel), *Spiniferites delicatus* (Sdel), *Spiniferites ristingensis* (Sris), Cysts of *Protoperidinium dalei* (Pdal)
	Sum outer neritic taxa (Cysts of phototrophs or mixotrophs)	*Spiniferites ramosus* (Sram) / *Spiniferites bulloideus* (Sbul), *Operculodinium centrocarpum* sensu Wall & Dale, 1966 (Ocen), *Spiniferites mirabilis* (Smir)
	Sum inner neritic taxa (Cysts of heterotrophs)	Cysts of *Protoperidinium nudum* (Pnud) / *Selenopemphix quanta* (Squa), Cysts of *Protoperidinium stellatum* (Pste), *Xandarodinium xanthum* (Xand)
POLLEN GROUPS	**Sum AP (arboreal taxa)**	Major taxa >2%: *Quercus, Corylus, Hedera, Betula, Ulmus, Tilia, Fagus* Minor taxa <2%: *Ilex, Carpinus, Prunus, Populus, Taxus, Abies, Viburnum, Juniperus, Ribes*
	Sum riparian trees	Major taxa >2%: *Alnus, Salix, Fraxinus*
	Non-indigenous trees	Major taxa >2%: *Castanea* Minor taxa <2%: *Vitis, Quercus ilex, Buxus, Juglans*
	Sum NAP (herbaceous taxa)	Major taxa >2%: Poaceae, Chenopodiaceae, Asteroideae, Brassicaceae, Cichorioideae, Cyperaceae, Ericaceae, *Lotus*, Juncaceae, *Plantago corronopus*, *Plantago* spp., Primulaceae, Ranunculaceae, *Saxifraga* Minor taxa <2%: *Sagittaria*, Amaryllidaceae, Apiaceae, Boraginaceae, Campanulaceae, *Centranthus*, *Spergula/Spergularia*, Caryophyllaceae, *Cistus*, *Sedum*,

		Crassulaceae, *Ephedra*, Euphorbiaceae, *Trifolium*, *Ulex*, Fabaceae, Gentianaceae, Geraniaceae, *Myriophyllum*, Iridaceae, *Lemna*, Liliaceae, *Papaver*, *Plantago maritima*, *Veronica*, *Armeria*, *Limonium*, *Potamogeton*, Oenotheraceae, Rosaceae, *Euphrasia*, Scrophulariaceae, *Typha/Sparganium*, Rubiaceae, *Viola*, *Hypericum*, *Polygonum*, Lamiaceae, *Althaenia*, *Helianthemum*, *Matthiola*, *Convolvulus*
	Sum ruderal and adventives	Major taxa >2%: *Rumex*, *Artemisia*, *Plantago lanceolata* Minor taxa <2%: *Mercurialis*, *Centaurea*, *Papaver*, Urticaceae
	Sum cultivated taxa	Major taxa >2%: *Cerealia*-type Minor taxa <2%: Cannabaceae

889

10. Figure captions

Figure 1: a) Map illustrating the general winter surface circulation in the Bay of Biscay (*Koutsikopoulos and Le Cann, 1996*; *Ferrer et al., 2009*), the repartition of muddy deposits on the shelf (*Allen and Castaing, 1977*), the location of the studied cores MD08-3204 CQ (Bay of Quiberon; *Baltzer et al., 2014*; I on the map a) and VK03-58bis (northern Grande Vasière, South Glénan islands; *Bourillet et al., 2005*, *2006*; *Naughton et al., 2007*; II on the map a) as well as other cited cores in the text, including GL3 (loc'h of Guidel; *Fernane et al., 2015*; 1 on the map a), CBT-CS11 (northern Grande Vasière, Penmarc'h sector; *Mojtahid et al., 2019*; *Penaud et al., 2020*; 2 on the map a), VC-08 (Bay of Douarnenez; *Lambert et al., 2019*; 3 on the map a) and MD95-2002 (Meriadzec Terrace; *Zumaque et al., 2017*; *Fersi et al., in prep.*; 4 on the map a). b) Surface sediment distribution over the South Armorican platform (*Lesueur and Klingebiel, 1986*; *Menier et al., 2014*) and location of the above mentioned inner to mid-shelf cores.

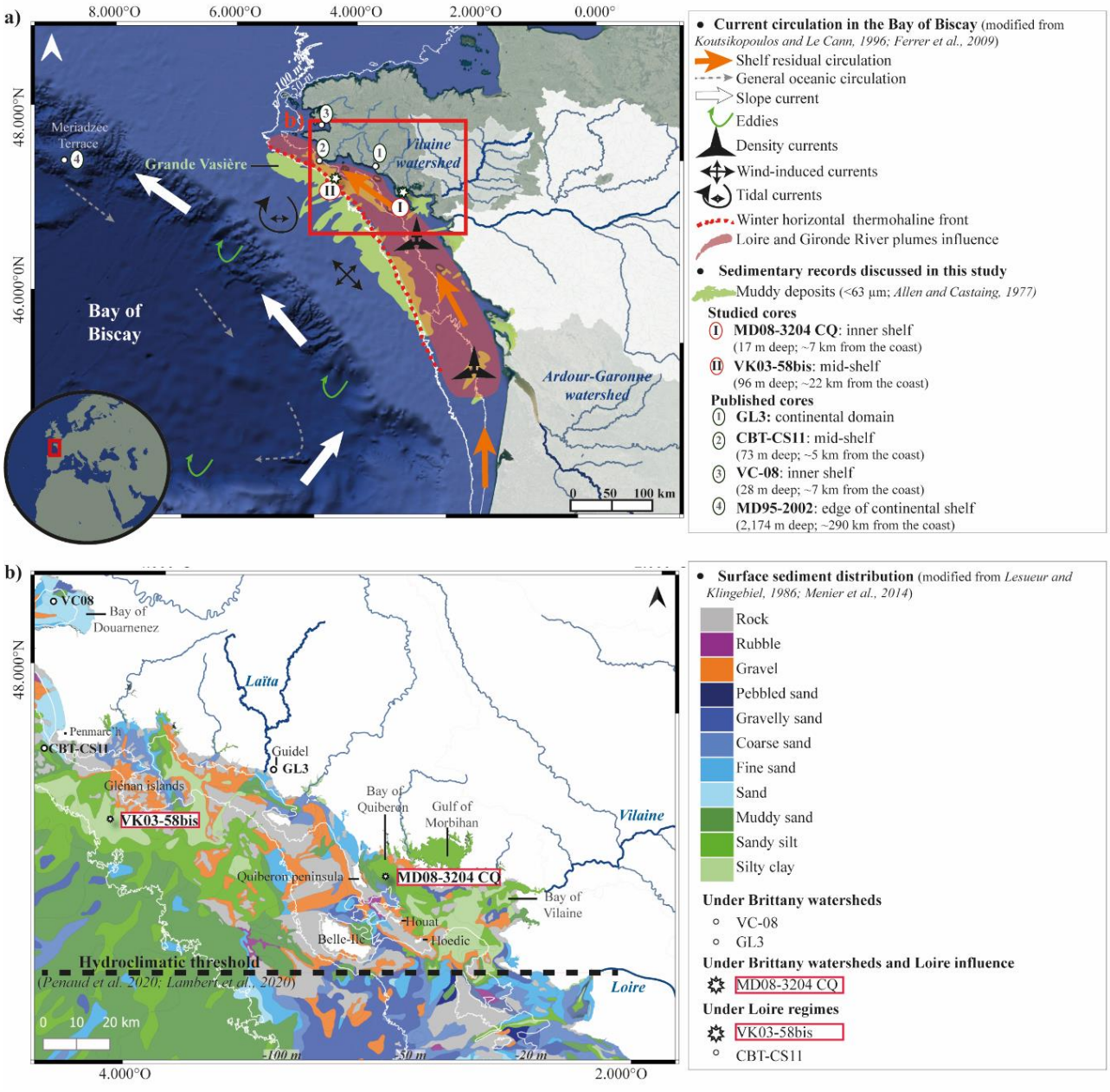


Figure 2: a) Age model of the studied core MD08-3204 CQ over the last 5.7 kyrs BP. b) Revised age models for cores CBT-CS11 (*Penaud et al., 2020*) and GL3 (*Fernane et al., 2015*). Age models were established using the rbacon package (*Blaauw and Christen, 2011*) in R version 4.1.2, and are expressed along cultural subdivisions for western Brittany (*Gorczynska et al., in prep*) and stratigraphical subdivisions (*Walker et al., 2019*).

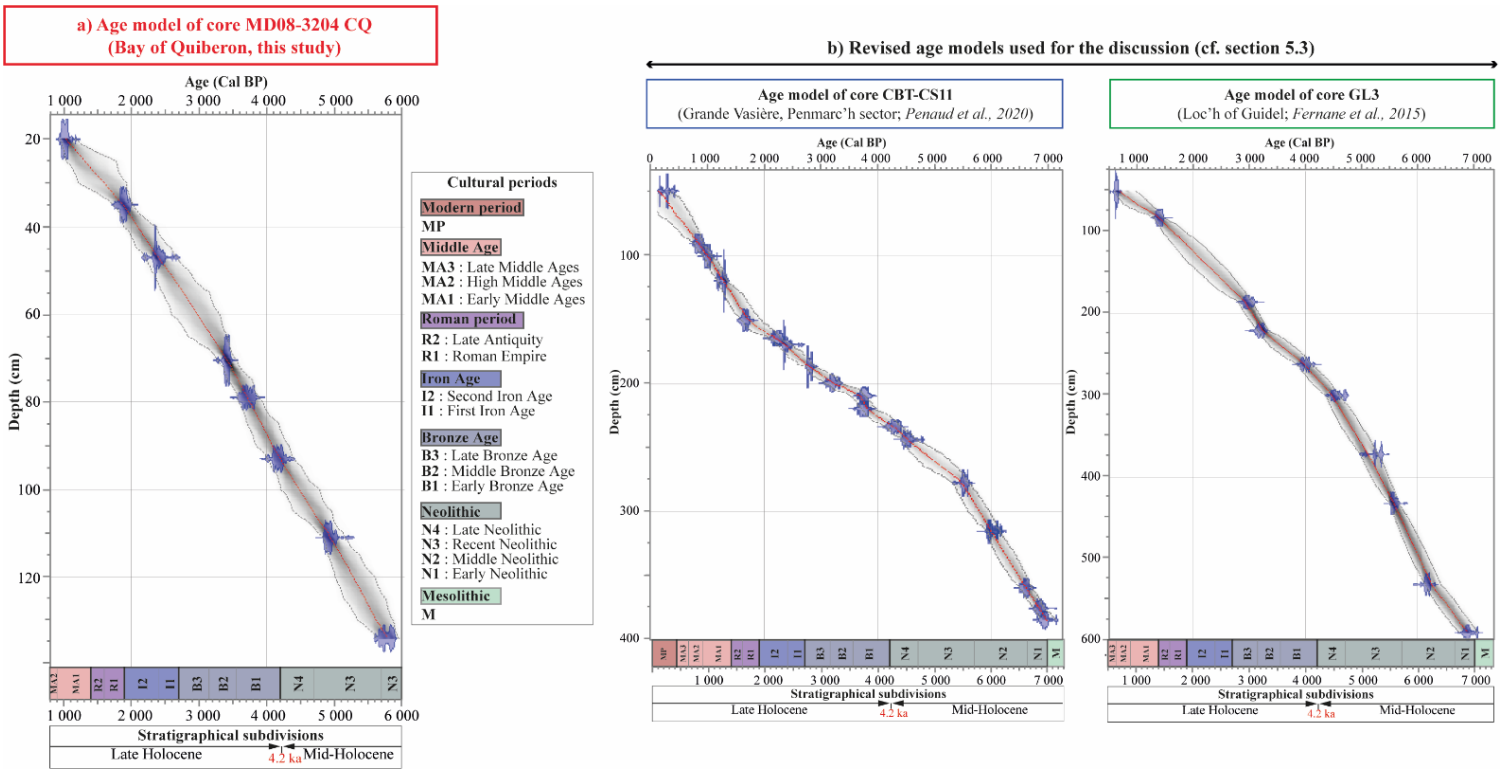


Figure 3: Sedimentological description for cores a) MD08-3204 CQ and b) VK03-58bis, including the logs for the description of the sedimentary facies (a and b), X-ray radiography (*Bourillet et al., 2005*; only b), the median grain-size analysis or D50 on total (a and b) and decarbonated (only b) sediments, grain-size distributions (regarding total sediments for a and decarbonated sediments for b), as well as Total Organic Carbon (TOC) measurements (only a). Age-depth plots for both cores (see Tables 1 and 2) are represented along sedimentation rates and the relative sea level (RSL) for southern Brittany (*García-Artola et al., 2018*). Intervals of low sedimentation rates linked to sediment remobilization and/or non-deposits are indicated using grey horizontal bands. HST: Highstand System Tract; TST: Transgressive System Tract; MFS: Maximum Flooding Surface.

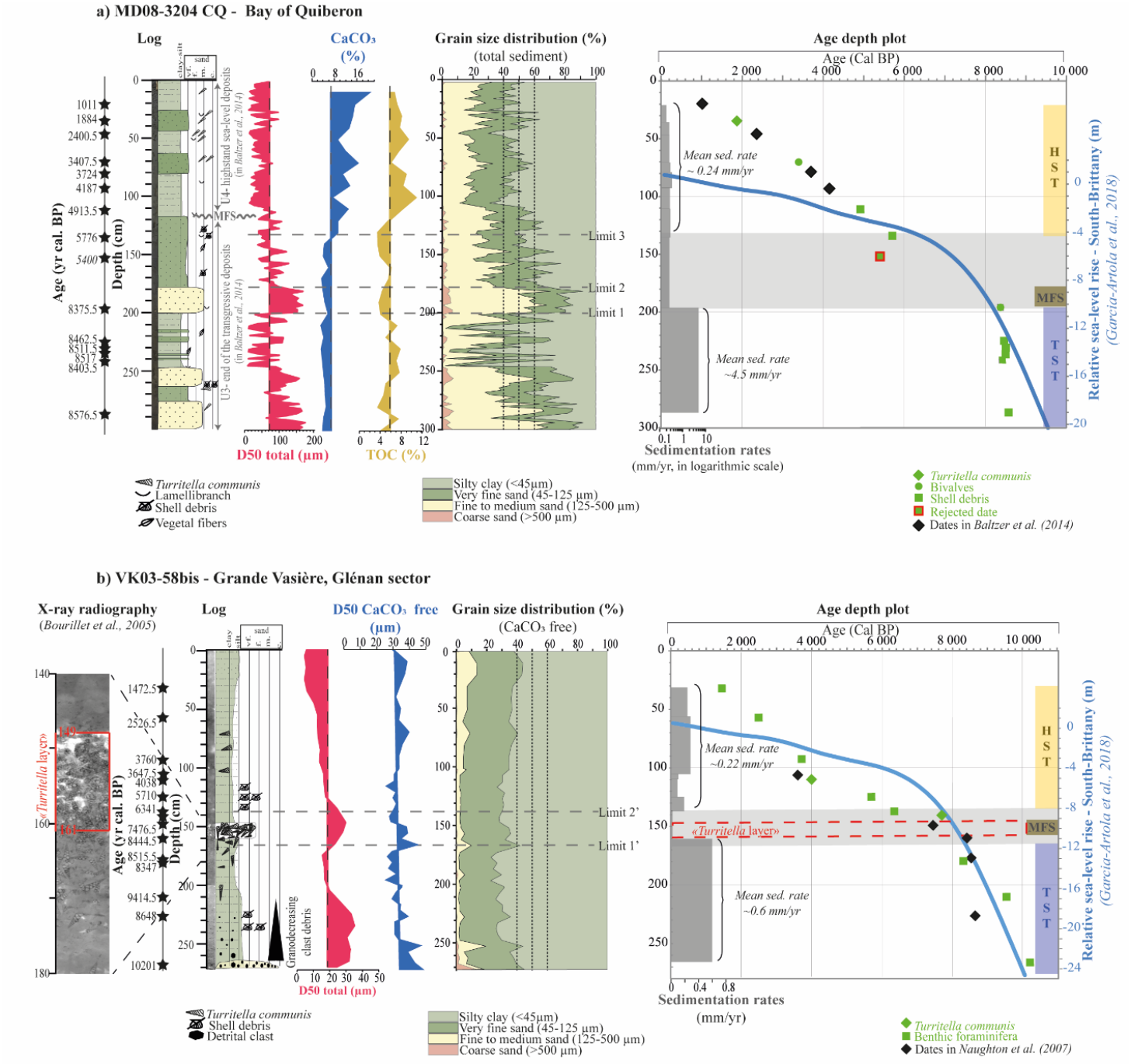


Figure 4: Along the log of core MD08-3204 CQ (see Fig. 3a): Palynological (dinocyst and pollen) data plotted vs. depth (cm) with concentrations (a and g), diversity Margalef indexes (b and h), number of different taxa (c and i), as well as dominance indexes (d and j) in parallel with percentages of the dominant species in dinocyst and pollen assemblages (e and k, respectively). Also, the number of counted specimens per analysed sample for pollen and dinocysts is highlighted in logarithmic scale allowing better visualizing the few number of dinocysts counted in the lower section of the MD08-3204CQ core. The interval of low sedimentation rates linked to sediment remobilization and/or non-deposits is indicated using a grey horizontal band (see Fig. 3a).

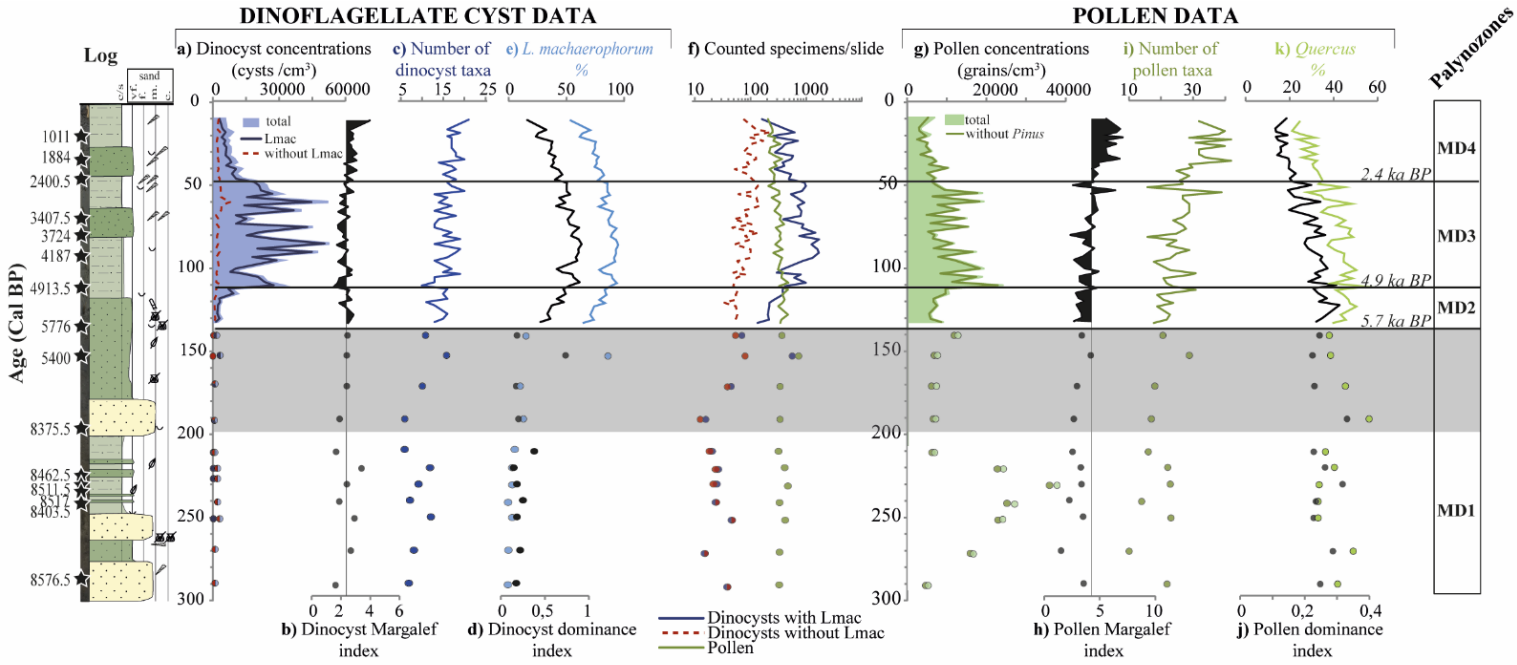


Figure 5: MD08-3204 CQ palynological data plotted vs. depth (cm). Major taxa (greater than 2% at least once in analyzed samples) of a) dinocyst and b) pollen assemblages. The interval of low sedimentation rates linked to sediment remobilization and/or non-deposits is indicating using grey horizontal bands (see Fig. 3a). Dinoflagellate cyst data are not represented for the latter interval, and they have been summed between 290 and 210 cm due to the extremely low dinocyst counts (see Fig 4). Regarding pollen data, points are represented in the grey band but will never be considered in the discussion. An average of the basal points will be considered for the discussion, as for dinocysts. Colored percentages highlight dinocyst and pollen groups (see Table 3).

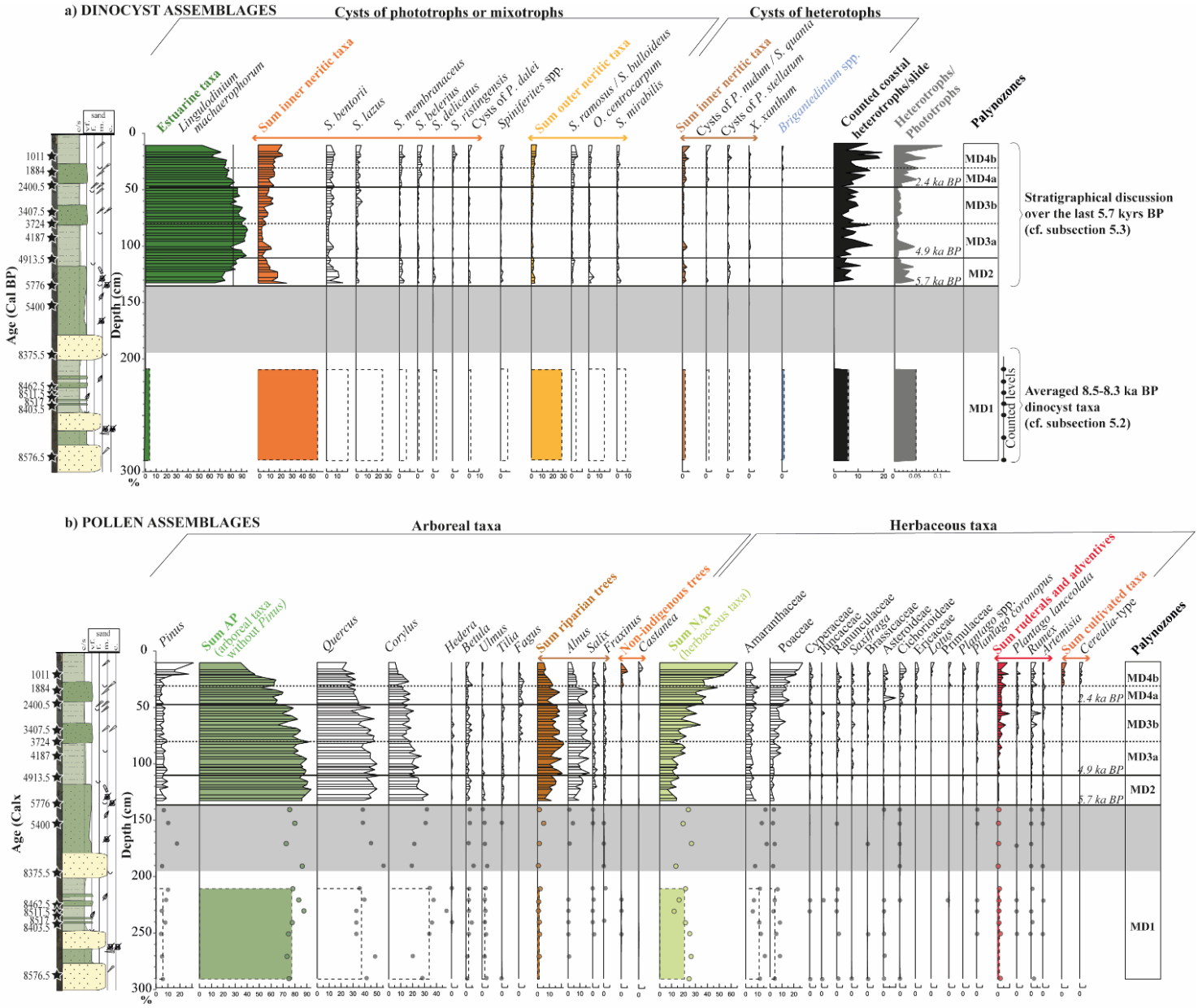


Figure 6: Conceptual model illustrating sedimentological configurations and main palynological tracers recorded at around 8.5 ka BP and from ~5.7 ka BP in the Bay of Quiberon. The number of palynomorphs represented in the two figures, respects the proportion of specimens counted for the two intervals (i.e., 8.5-8.3 ka BP and 5.7-1 ka BP) and are based on an arbitrary initial value of 4 grains of *Quercus* for the interval 5.7-1 ka BP. On both intervals dinocyst group (see Table 3; Fig. 5) percentages were also averaged.

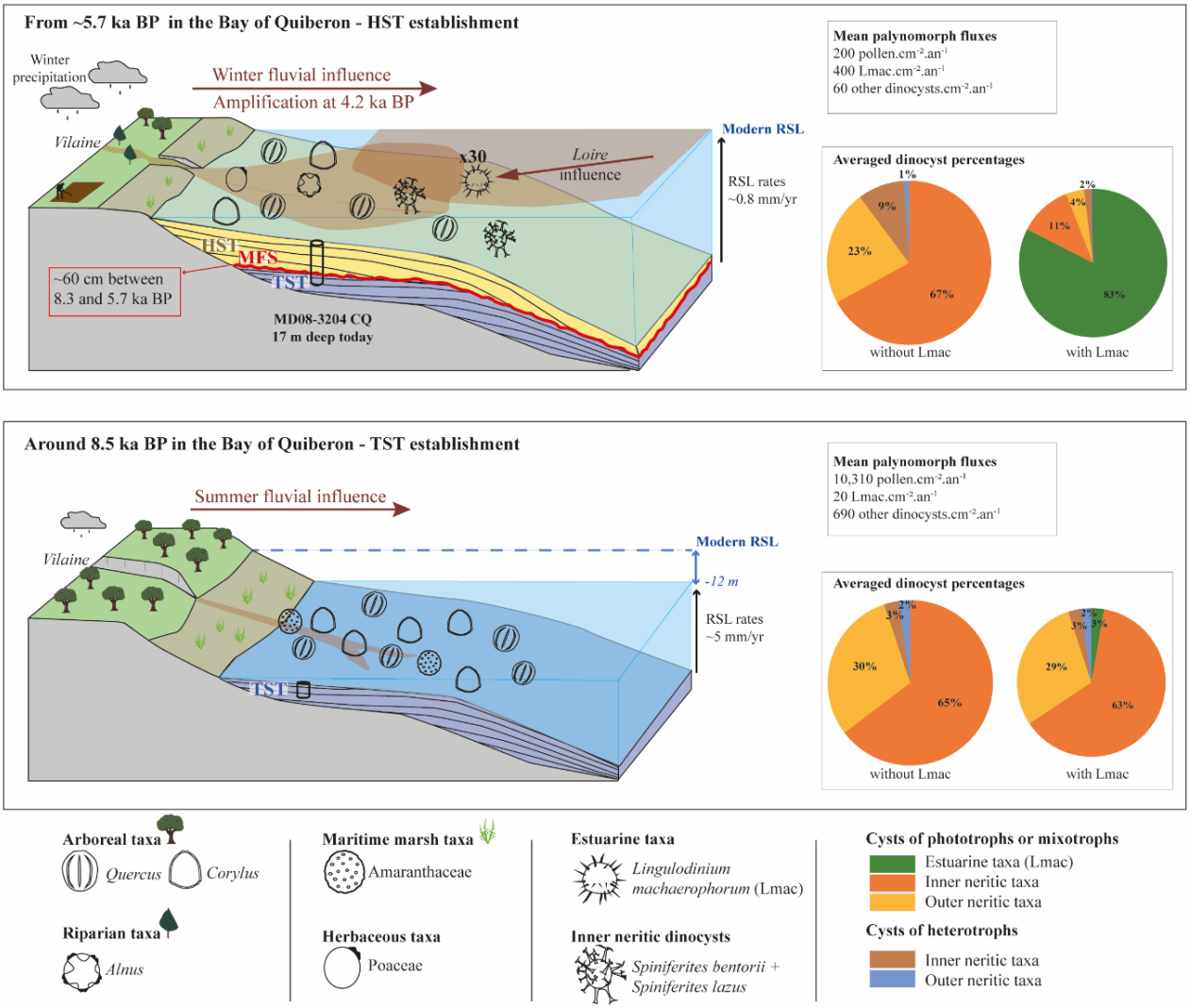


Figure 7: 8.5–8.3 ka BP averaged palynomorph (a) and dinocyst (b) data (~200 yrs) along an inshore-offshore gradient with two proximal cores (MD08-3204 CQ, Bay of Quiberon, this study; and VC-08, Bay of Douarnenez, *Lambert et al., 2019*) and two distal cores (VK03-58bis, Grande Vasière, Glénan sector, *Naughton et al., 2007*; *Penaud, pers. comm.*; and MD95-2002, Meriadzec Terrace, *Zumaque et al., 2017*; *Fersi, et al., in prep.*). See Fig. 1 for core locations.

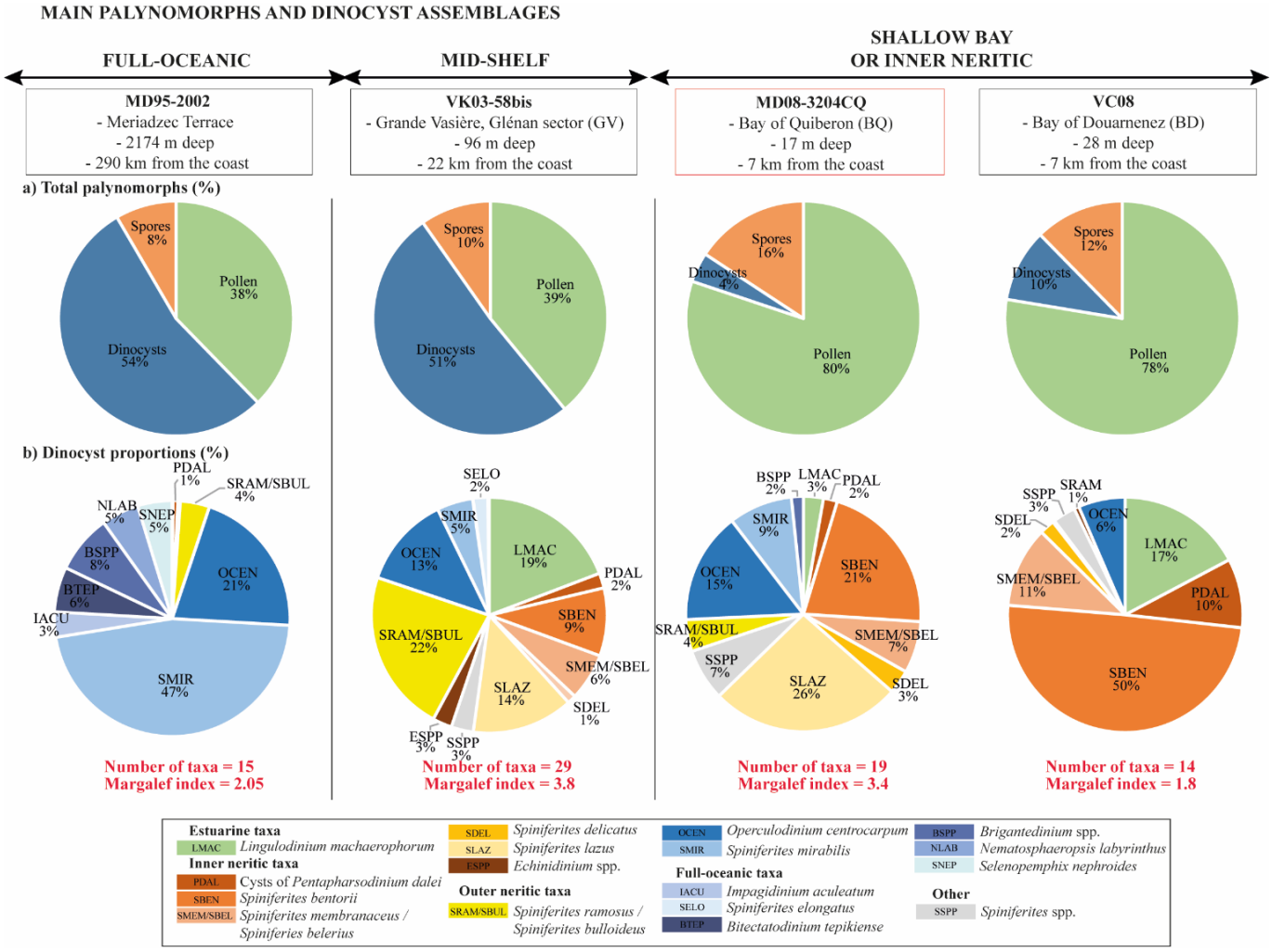
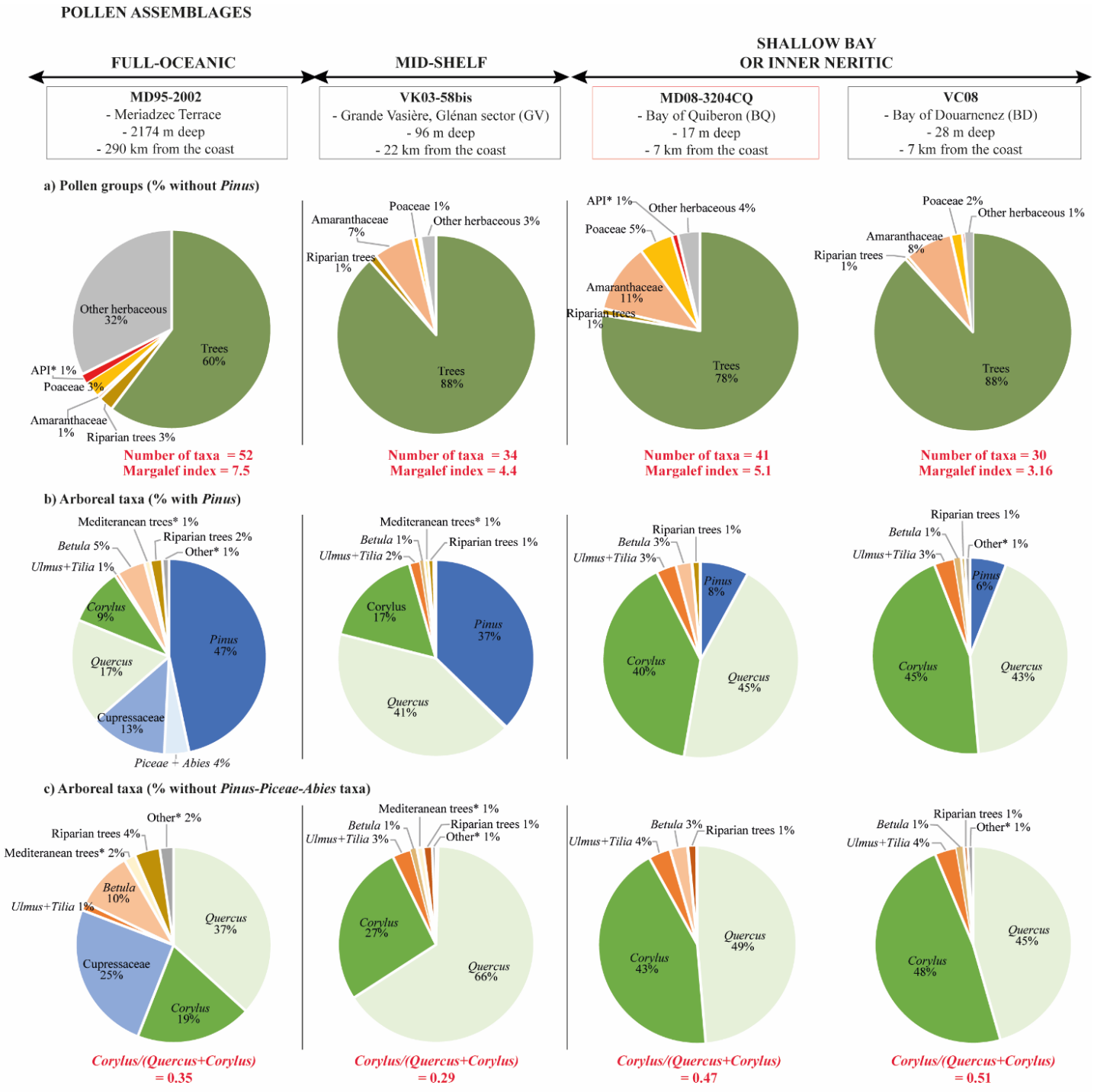


Figure 8: 8.5–8.3 ka BP averaged pollen data (~200 yrs) along an inshore-offshore gradient with two proximal cores (MD08-3204 CQ, Bay of Quiberon, this study; and VC-08, Bay of Douarnenez, *Lambert et al., 2019*) and two distal cores (VK03-58bis, Grande Vasière, Glénan sector, *Naughton et al., 2007*; *Penaud, pers. comm.*; and MD95-2002, Meriadzec Terrace, *Zumaque et al., 2017*; *Fersi, et al., in prep.*). See Fig. 1 for core locations.



API*: Cannabaceae, *Cerealia*-type, *Plantago lanceolata*, *Centaurea*, *Rumex* / **Mediteranean trees***: *Quercus suber, Quercus ilex* /
Other* : main sum taxa <2%

Figure 9: Selected palynological data (i.e., *Lingulodinium machaerophorum*, *Alnus*, *Quercus*, *Corylus*, Poaceae) acquired on cores MD08-3204 CQ (in orange; this study), CBT-CS11 (in blue; Penaud et al., 2020) and GL3 (in green; *Fernane et al., 2015*) addressed in parallel with stratigraphical and cultural subdivisions (see Fig. 2). Note the additional sedimentological data from core CBT-CS11 (i.e., D50 grain size on decarbonated sediments; *Mojtahid et al., 2019*) in order to discuss the load-transport capacity of the Loire river. Straight horizontal lines correspond to limits between MD08-3204 CQ palynozones. Dotted horizontal lines correspond to hydrodynamic (4.2 and 3.3 ka BP) or anthropogenic (1.2 ka BP) thresholds previously identified (*Penaud et al., 2020*).

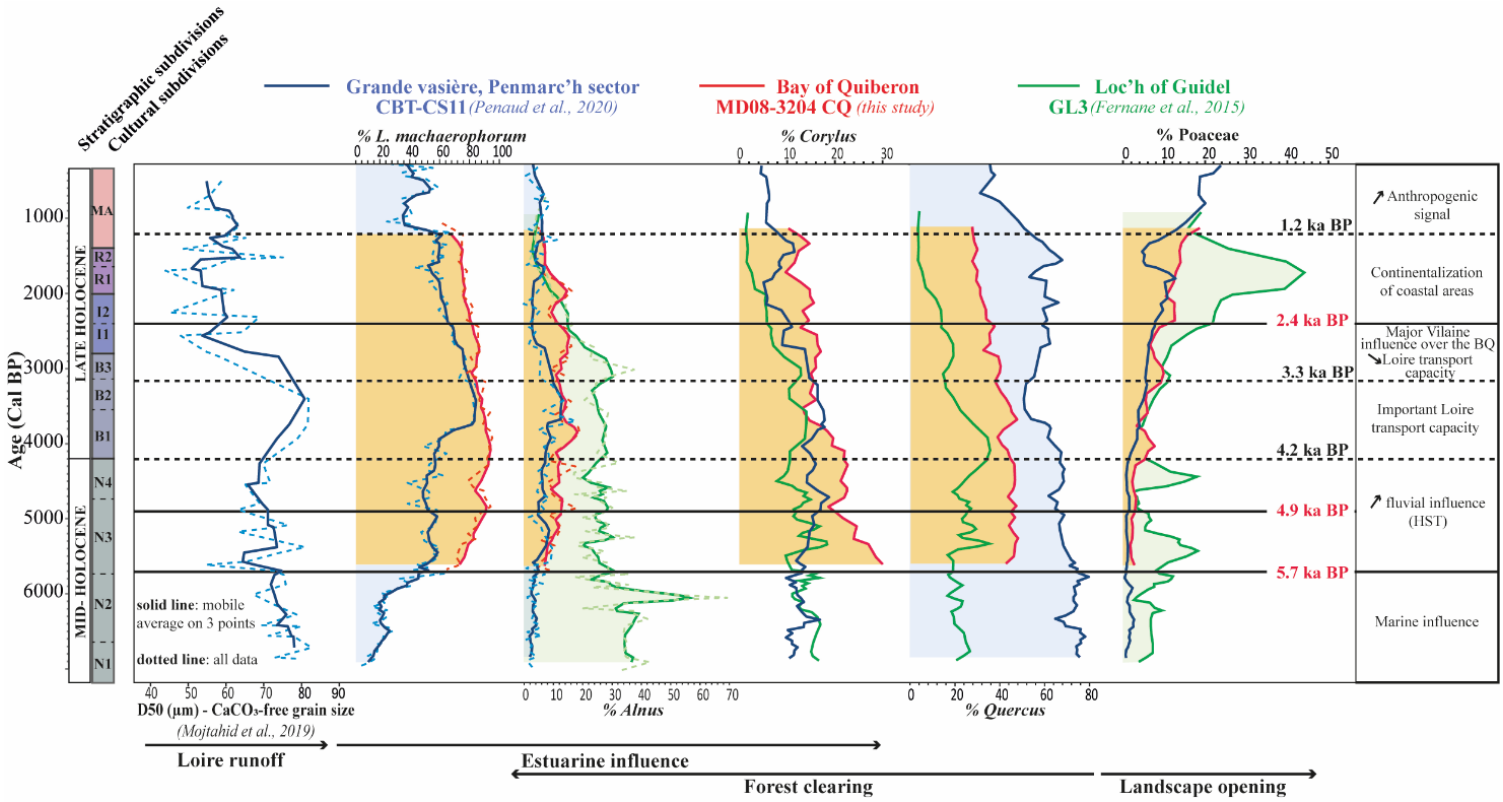
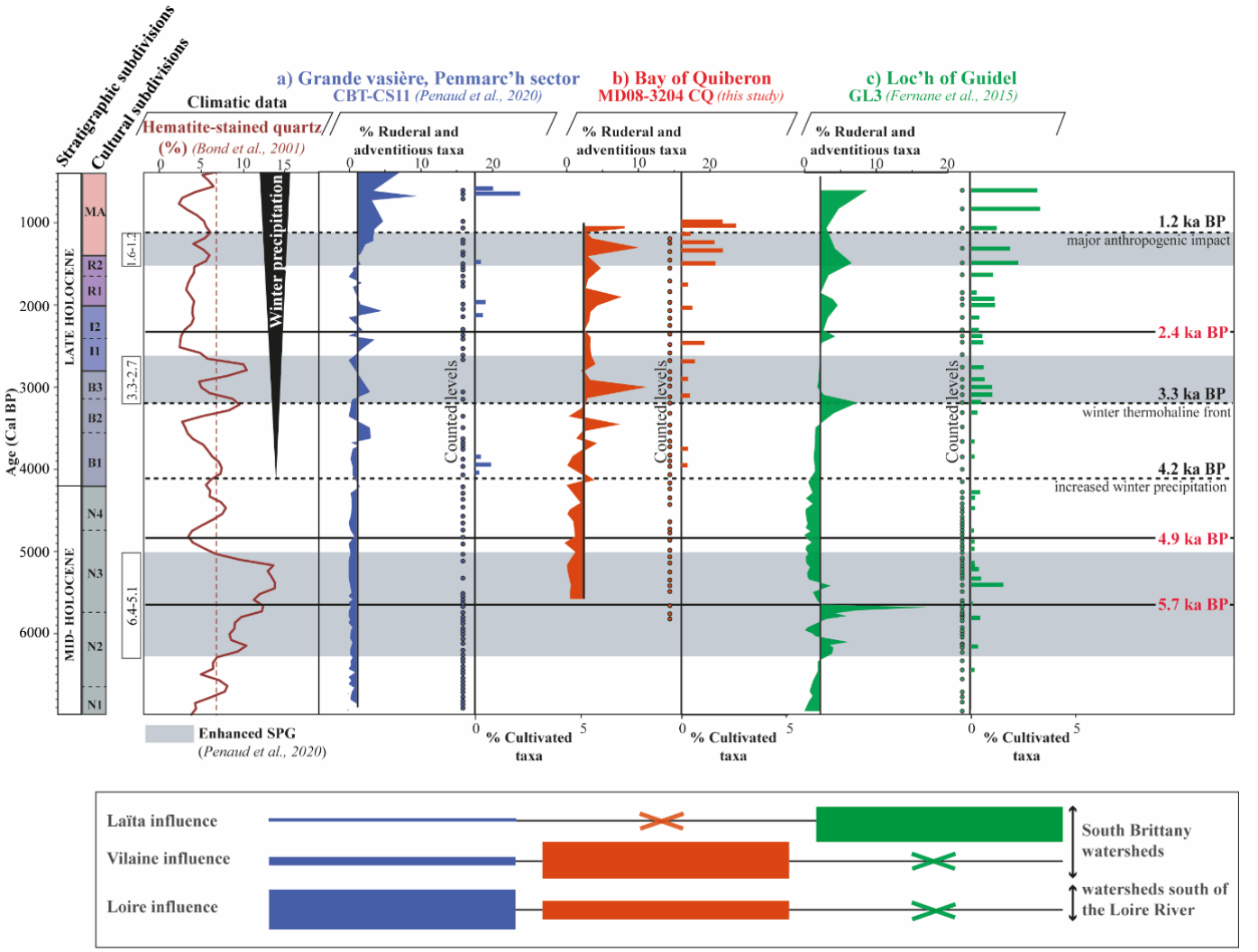


Figure 10: Anthropogenic Pollen Indicators (API: ruderal and adventitious taxa, cultivated taxa; see Table 3) calculated for cores MD08-3204 CQ (in orange; this study), CBT-CS11 (in blue; *Penaud et al., 2020*), and GL3 (in green; *Fernane et al., 2015*). Palynological data are addressed in parallel with periods of subpolar gyre (SPG) strengthening (cf. *Penaud et al., 2020*), represented using grey horizontal bands. See Fig. 1 for core and rivers locations, as well as Fig. 2 for cultural subdivisions. Straight horizontal lines correspond to limits between MD08-3204 CQ palynozones. Dotted horizontal lines correspond to hydrodynamic (4.2 and 3.3 ka BP) or anthropogenic (1.2 ka BP) thresholds previously identified (*Penaud et al., 2020*).



11. References

Allen, G.P., Castaing, P., 1977. Carte de répartition des sédiments superficiels sur le plateau continental du Golfe de Gascogne. Bull. Inst. Géol. Bassin d'Aquitaine, 21, 255–261.

Alley, R.B., Marotzke, J., Nordhaus, W.D., Overpeck, J.T., Peteet, D.M., Pielke, R.A., Pierrehumbert, R.T., Jr, Rhines, P.B., Stocker, T.F., Talley, L.D., Wallace, J.M. 2003. Abrupt climate change. Science, 299, 2005–2010. doi/10.1126/science.1081056

Andreieff, P., Bouysse, P., Châteauneuf, J.-J., L'Homer, A., Scolari, G., 1971. La couverture sédimentaire meuble du plateau continental externe de la Bretagne méridionale (Nord du golfe de Gascogne). Cahiers Océanographiques, 23, 343–381.

Arthuis, R., Goubert, E., Nauleau, J.F., 2015. Essai de reconstitution paléogéographique de la Loire par l'étude de la documentation existante. In "L'environnement en mémoire: marqueurs, outils et perspectives, Bardot-Cambot & Tranoy (coord), Ed. Presses Universitaires de Rennes, 75–88.

Arthuis, R., 2020. Les changements hydromorphologiques de l'estuaire de la Loire et l'évolution du port de Rezé/Ratiatum (Loire-Atlantique). Gallia, 77-1, 55–66. https://doi.org/10.4000/gallia.5317

Ayache, M., Swingedouw, D., Mary, Y., Eynaud, F., Colin, C., 2018. Multi-centennial variability of the AMOC Over the Holocene: A New Reconstruction Based on Multiple Proxy-derived SST Records. Glob. Planet. Change 170, 172-189. https://doi.org/10.1016/j.gloplacha.2018.08.016

Baltzer, A., Walter-Simonnet, A.-V., Mokeddem, Z., Tessier, B., Goubert, E., Cassen, S., Diffo, A., 2014. Climatically-driven impacts on sedimentation processes in the Bay of Quiberon (south-Brittany, France) over the last 10,000 years. Holocene, 24, 679–688. https://doi.org/10.1177/0959683614526933

Baltzer, A., Mokeddem, Z., Goubert, E., Larteaud, F., Labourdette, N., Fournier, J., Bourillet, J.-F., 2015. The "*Turritella* Layer": A Potential Proxy of a Drastic Holocene Environmental Change on the North–East Atlantic Coast. In: Maanan M., Robin M. (eds) Sediment Fluxes in Coastal Areas. Coastal Research Library, vol 10. Springer, Dordrecht. https://doi.org/10.1007/978-94-017-9260-8_1

Bassinot, F.C, Labeyrie, L.D., 1996. IMAGES - MD 101 à bord du Marion-Dufresne du 29 mai au 11 juillet 1995. A coring cruise of the R/V Marion Dufresne in the North Atlantic Ocean and Norwegian Sea. Les Publications de l'Institut français pour la recherche et la technologie polaires. Les Rapports des campagnes à la mer, (96-1), 221p. https://archimer.ifremer.fr/doc/00633/74461/

Barbier, D., 1999. Histoire de la végétation du nord-mayennais, de la fin du Weichsélien à l'aube du XXIe siècle. Mise en évidence d'un Tardiglaciaire armoricain. Interactions homme/milieu, Groupe d'Études des Milieux Naturels, t. 1, texte, 285 p., t. 2, illustrations, 62 p., Nantes.

Benito, G., Macklin, M.G., Zielhofer, C., Jones, A.F., Machado, M.J., 2015. Holocene flooding and climate change in the Mediterranean. Catena, 130, 13-33. https://doi.org/10.1016/j.catena.2014.11.014

Bennet, K.D., 1992. Psimpoll- Quickbasic Program That Generates Postscript Page Description of Pollen Diagrams. INQUA Commission for the Study of the Holocene: Working Group on Data-Handling Methods, Newsletter 8, 11–12.

Bégeot, C., 1998. Le comportement pollinique du Noisetier (*Corylus avellana*), son rôle comme indicateur d'impacts anthropiques ? L'exemple d'un transect dans le sud du Jura. Acta bot. Gallica, 145 (4), 271–277. https://doi.org/10.1080/12538078.1998.10516307

Berger, A., Loutre, M.F., 1991. Insolation values for the climate of the last 10 million years. Quat. Sci. Rev. 10 (4), 297–317. https://doi.org/10.1016/0277-3791(91)90033-Q

Beug, H.-J., 1961. Beiträge Zur Postglazialen Floren- Und Vegetationsgeschichte in Süddalmatien: Der See „Malo Jezero" Auf Mljet: Teil I: Vegetationsentwicklung. Flora Oder Allg. Bot. Ztg. 150 (4), 600–631. https://doi.org/10.1016/S0367-1615(17)33232-9

Blaauw, M., Christen, J.A., 2011. Flexible paleoclimate age-depth models using an autoregressive gamma process. Bayesian Anal. 6 (3), 457–474. DOI: 10.1214/11-BA618

Blamart D., Baltzer, A., Volker, A., 2008. MD 169 / MICROSYSTEMS cruise, RV Marion Dufresne, https://doi.org/10.17600/8200100.

Blott, S.J. and Pye, K., 2001. GRADISTAT: a grain size distribution and statistics package for the analysis of unconsolidated sediments. Earth Surface Processes and Landforms, 26, 1237–1248. https://doi.org/10.1002/esp.261

Bond, G., Showers, W., Cheseby, M., Lotti, R., Almasi, P., deMenocal, P., Priore, P., Cullen, H., Hajdas, I., Bonani, G., 1997. A pervasive millenial-scale cycle in North Atlantic Holocene and glacial climates. Science, 278, 1257–1266. https://doi.org/10.1126/science.278.5341.1257

Bond, G., Kromer, B., Beer, J., Muscheler, R., Evans, M., Showers, W., Hoffmann, S., LottiBond, R., Hajdas, I., Bonani, G. 2001. Persistent solar influence on North Atlantic climate during the Holocene. Science, 294, 2130–36. https://doi.org/10.1126/science.1065680

Bourillet, J-F., Dubrulle, C., Goubert, E., Jouanneau, J-M., Cortij, E., Weber, O., Lesueur, P., 2005. La Grande Vasière : architecture, mise en place et estimation des facteurs de son évolution. Colloque Golfe de Gascogne. 22-24 mars 2005, Brest. https://archimer.ifremer.fr/doc/00749/86127/

Bourillet, J-F., Jouanneau, J-M., Macher, C., Le Hir, P., Naughton, F., 2006. "La Grande Vasière" mid-shelf mud belt: Holocene sedimentary structure, natural and anthropogenic impact. In Abstracts of the X International Symposium on Oceanography of the Bay of Biscay. Vigo, Spain, 19-21 April 2006, 131–134. https://archimer.ifremer.fr/doc/00000/6243/

Broström, A., Nielsen, A.B., Gaillard, M.-J., Hjelle, K., Mazier, F., Binney, H., Bunting, J., Fyfe, R., Meltsov, V., Poska, A., 2008. Pollen productivity estimates of key European plant taxa for quantitative reconstruction of past vegetation: a review. Veg. Hist. Archaeobotany, 17, 461–478. https://doi.org/10.1007/s00334-008-0148-8

Carter, M.C., 2008. *Turritella communis* An auger shell. In Tyler-Walters H. and Hiscock K. (eds) Marine Life Information Network : Biology and Sensitivity Key Information Reviews, [on-line]. Plymouth: Marine Biological Association of the United Kingdom.

Castaing, P., Allen, G.P., 1981. Mechanisms controlling seaward escape of suspended sediment from the Gironde: A macrotidal estuary in France. Mar. Geol. 40(1), 101–118. https://doi.org/10.1016/0025-3227(81)90045-1

Castaing, P., Froidefond, J.M., Lazure, P., Weber, O., Prud'homme, R., Jouanneau, J.M., 1999. Relationship between hydrology and seasonal distribution of suspended sediments on the continental shelf of the Bay of Biscay. Deep Sea Research Part II: Topical Studies in Oceanography 46(10), 1979-2001. https://doi.org/10.1016/S0967-0645(99)00052-1

Castanet C., 2008. La Loire en val d'Orléans. Dynamiques fluviales et socio-environnementales durant les derniers 30 000 ans : de l'hydrosystème à l'anthroposystème, Thèse de doctorat, Université de Paris-1 Panthéon-Sorbonne, 549 p.

Charria, G., Lazure, P., Le Cann, B., Serpette, A., Reverdin, G., Louazel, S., Batifoulier, F., Dumas, F.,

Pichon, A., Morel, Y., 2013. Surface layer circulation derived from Lagrangian drifters in the Bay of Biscay. J. Mar; Syst., S60-S76. DOI: 10.1016/j.jmarsys.2011.09.015

Charria, G., 2018. Evolutions interannuelles de la circulation dans le golfe de Gascogne - vers une dynamique à (sous)mésoéchelle en milieu côtier. Observer et simuler un océan côtier turbulent. HDR. https://archimer.ifremer.fr/doc/00475/58702/

Chaumillon, E., Proust, J.-N., Menier, D., Weber, N, 2008. Incised-valley morphologies and sedimentary-fills within the inner shelf of the Bay of Biscay (France): a synthesis. J. Mar. Syst., 72, 383-396. https://doi.org/10.1016/j.jmarsys.2007.05.014

Costoya, X., Fernandez-Novoa, D., deCastro, M., Santos, F., Lazure, P., Gomez-Gesteira, M., 2016. Modulation of sea surface temperature warming in the Bay of Biscay by Loire et Gironde Rivers. J. Geophys. Res. Oceans, 120, 14 p. https://doi.org/10.1002/2015JC011157

Cyprien, A.L., 2002. Chronologie de l'interaction de l'homme et du milieu dans l'espace central et aval de la Loire (Ouest de la France). Thèse doctorat, Université de Nantes, Tome I, 183 pp ; Tome II, 75 pp.

Delaine, M., Châtelet, E., Bout-Roumazeilles, V., Goubert, E., Le Cadre, E., Recourt, P., Trentesaux, A., Arthuis, R., 2015. Multiproxy approach for Holocene paleoenvironmental reconstructions from microorganisms (testate amoebae and foraminifera) and sediment analyses: The infilling of the Loire Valley in Nantes (France). Holocene 25, 407–420. https://doi.org/10.1177/0959683614561883

de Vernal, A., Henry, M., Bilodeau, G., 1999. Technique de préparation et d'analyse en micropaléontologie. Les Cahiers du GEOTOP vol. 3, Université du Québec à Montréal, Montréal, Canada.

de Vernal, A., Radi, T., Zaragosi, S., Van Nieuwenhove, N., Rochon, A., Allan, E., De Schepper, S., Eunaud, F., Head, M.J., Limoges, A., Londeix, S., Marret, F., Matthiessen, J., Penaud, A., Pospelova, V., Price, A., Richerol, T., 2020. Distribution of common modern dinoflagellate cyst taxa in surface sediments of the Northern Hemisphere in relation to environmental parameters: The new n= 1968 database. Mar. Micropaleontol., 159, 101796. https://doi.org/10.1016/j.marmicro.2019.101796

Dubrulle, C., Jouanneau, J.M., Lesueur, P., Bourillet, J.F., Weber, O., 2007. Nature and rates of fine-sedimentation on a mid-shelf: "La Grande Vasière" (Bay of Biscay, France). Cont. Shelf Res. 27, 2099-2115. https://doi.org/10.1016/j.csr.2007.05.002

1118 Dussud, L., 2010. CABTEX cruise, RV Pourquoi pas ? https://doi.org/10.176 00/10030050.
1119
1120 Engelhart, S.E., Horton, B.P., 2012. Holocene sea level database for the Atlantic coast of the United
1121 State. Quat. Sci. Rev. 54, 12–25. https://doi.org/10.1016/j.quascirev.2011.09.013
1122
1123 Fatela, F., Taborda, R., 2002. Confidence limits of species proportions in microfossil assemblages. Mar.
1124 Micropaleontol. 45, 169–174. https://doi.org/10.1016/S0377-8398(02)00021-X
1125
1126 Fernane, A., Gandouin, E., Penaud, A., Van Vliet-Lanoë, B., Goslin, J., Vidal, M., Delacourt, C., 2014.
1127 Coastal palaeoenvironmental record of the last 7 ka BP in NW France: sub-millenary climatic and
1128 anthropic Holocene signals. Holocene 24, 1785–1797. https://doi.org/10.1177%2F0959683614551223
1129
1130 Fernane, A., Penaud, A., Gandouin, E., Goslin, J., Van Vliet-Lanoë, B., Vidal, M., 2015. Climate
1131 variability and storm impacts as major drivers for human coastal marsh withdrawal over the Neolithic
1132 period (Southern Brittany, NW France). Palaeogeogr., Palaeoclimatol., Palaeoecol. 435, 136–144.
1133 https://doi.org/10.1016/j.palaeo.2015.05.029
1134
1135 Ferrer, L., Fontán, A., Mader, J., Chust, G., González, M., Valencia, V., Uriarte, Ad., Collins, M. B.,
1136 2009. Low-salinity plumes in the oceanic region of the Basque Country. Continental Shelf Research,
1137 29, 8, 970–984. DOI: 10.1016/j.csr.2008.12.014.
1138
1139 Fersi, W., Penaud, A., David, O., Lambert, C., Vidal, M., Stéphan, P., Zumaque, J., De Vernal, A.,
1140 Eynaud, F., in prep. Paleoenvironmental signature of Holocene records from the northern margin of the
1141 Bay of Biscay.
1142
1143 Folliot, B., 2004. La Grande Vasière : Etude sédimentologique de deux secteurs septentrionaux. Rapport
1144 de DEA Dynamique et Environnements Sédimentaires, Université Lille-Caen-Rouen, p.39.
1145
1146 Fujiwara, O., Kamataki, T., Masuda, F., 2004. Sedimentological time-averaging and 14C dating of
1147 marine shells. Nucl. Instrum. Methods Phys. Res., B Beam Interact. Mater. Atoms 223–224, 540–544.
1148 https://doi.org/10.1016/j.nimb.2004.04.101
1149
1150 Funder, S., Demidov, I., Yelovicheva, Y., 2002. Hydrography and mollusc faunas of the Baltic and the
1151 White Sea–North Sea seaway in the Eemian. Palaeogeogr., Palaeoclimatol., Palaeoecol.184, 275–304.
1152 http://dx.doi.org/10.1016/S0031-0182(02)00256-0
1153

Ganne, A., Leroyer, C., Penaud, A., Mojtahid, M., 2016. Present-day palynomorph deposits in an estuarine context: the case of the Loire Estuary. J. Sea Res. 118, 35–51. https://doi.org/10.1016/j.seares.2016.10.006

García-Artola, A., Stéphan, P., Cearreta, A., Kopp, R.E., Khan, N.S., Horton, B.P., 2018. Holocene sea-level database from the Atlantic coast of Europe. Quat. Sci. Rev. 196, 177–192. https://doi.org/10.1016/j.quascirev.2018.07.031

García-Mozo, H., Galán, C., Jato, V., Belmonte, J., 2006. *Quercus* pollen season dynamics in the Iberian peninsula: response to meteorological parameters and possible consequences of climate change. Ann. Agric. Environ. Med.13, 209–224.

Gaudin, L., 2004. Transformations spatio-temporelles de la végétation du nord-ouest de la France depuis la fin de la dernière glaciation. Reconstitutions paléo-paysagères. Thèse doctorat, Université de Rennes I, 660 pp. https://tel.archives-ouvertes.fr/tel-00470150

Giraudeau, J., Grelaud, M., Solignac, S., Andrews, J., Moros, M., Jansen, E., 2010. Millennial scale variability in Atlantic water advection to the Nordic seas derived from Holocene coccolith concentration records. Quat. Sci. Rev. 29, 1276–1287. https://doi.org/10.1016/j.quascirev.2010.02.014

Goslin, J., Van Vliet Lanoë, B., Spada, G., Bradley, S., Tarasov, L., Neil, S. and Suanez, S., 2015. A new Holocene relative sea-level curve for western Brittany (France): Insights on Isostatic dynamics along the Atlantic coasts of north-western Europe. Quat. Sci. Rev. 129, 341–365. https://doi.org/10.1016/j.quascirev.2015.10.029

Goslin, J., Fruergaard, M., Sander, L., Gałka, M., Menviel, L., Monkenbusch, J., Thibault, N., Clemmensen, L.B., 2018. Holocene centennial to millennial shifts in North-Atlantic storminess and ocean dynamics. Sci. Rep. 8, 12778. https://doi.org/10.1016/j.quascirev.2015.10.029

Gorczynska, A., Stéphan, P., Pailler, Y., Nicolas, C., Penaud, A., David, O., Vidal, M., Le Gall, B., submitted, in prep. Holocene evolution of coastal dunes in western France: regional reconstruction from archaeological and historical data. Aeolian Research.

Gregoire, G., Le Roy, P., Ehrhold, A., Jouet, G., and Garlan, T. 2017. Control factors of Holocene sedimentary infilling in a semi-closed tidal estuarine-like system: the bay of Brest (France). Mar. Geol. 385, 84–100. https://doi.org/10.1016/j.margeo.2016.11.005

Guilcher, A., 1948. Le relief de la Bretagne méridionale de la baie de Douarnenez à la Vilaine. PhD Thesis, Paris, H. Potier (Ed.), La Roche-sur-Yvon. 682 p.

Guillaud, J., Aminot, A., Delmas, D., Gohin, F., Lunven, M., Labry, C., Herbland, A., 2008. Seasonal variation of riverine nutrient inputs in the northern Bay of Biscay (France), and patterns of marine phytoplankton response. J. Mar. Syst. 72, 309–319. https://doi.org/10.1016/j.jmarsys.2007.03.010

Hammer, Ø., Harper, D.A.T., Paul, D.R., 2001. Past: Paleontological Statistics Software Package for Education and Data Analysis. Paleontologia Electronica, 4, 1, 9 p.

Hátún, H., Sandø, A. B., Drange, H., Hansen, B., Valdimarsson, H., 2005. Influence of the Atlantic subpolar gyre on the thermohaline circulation. Science 309, 1841–1844. DOI: 10.1126/science.1114777

Heiri, O., Lotter, A.F., Lemcke, G., 2001. Loss on ignition as a method for estimating organic and carbonate content in sediments: reproducibility and comparability of results. Journal of paleolimnology, 25, 101–110. https://doi-org.scd-proxy.univ-brest.fr/10.1023/A:1008119611481

Holmes, P., 1994. The sorting of spores and pollen by water: experimental and field evidence. In: Traverse, A. (Ed.), Sedimentation of Organic Particles. Cambridge University Press, Cambridge, 9–32.

Hurrell, JW, 1995. Decadal trends in the North Atlantic Oscillation: regional temperatures and precipitation. Science 269, 676–679. DOI: 10.1126/science.269.5224.676

Hurrell, J.W,, Kushnir, Y., Ottersen, G., Visbeck, M., 2003. The North Atlantic Oscillation: climate significance and environmental impacts. Geophys. Monogr. Ser. 134, 279.

Joly, C., Visset, L., 2009. Evolution of vegetation landscapes since the Late Mesolithic on the French West Atlantic coast. Rev. Palaeobot. Palynol. 154, 124–179.. https://doi.org/10.1016/j.revpalbo.2008.12.011

Jouanneau, J.-M., Weber, O., Cremer, M., Castaing, P., 1999. Fine-grained sediment budget on the continental margin of the Bay of Biscay. Deep-Sea Res., II, 46, 2205–2220. https://doi.org/10.1016/S0967-0645(99)00060-0

Jouet, G., Augris, C., Hallegouët, B., Le Roy, P., Rolet, J., 2003. La vallée d'Ys: un paléoréseau hydrographique immerge en baie de Douarnenez (Finistère, France). Compt. Rendus Geosci. 335 (5), 487–494. https://doi.org/10.1016/S1631-0713(03)00066-X

Kidwell, S.M., 1997. Time-Averaging in the Marine Fossilrecord: Overview of Strategies and Uncertainties. Geobios, 30 (7), 977–995. https://doi.org/10.1016/S0016-6995(97)80219-7

Koutsikopoulos, C., Le Cann, B., 1996. Physical processes and hydrological structures related to the Bay of Biscay anchovy. Sci. Mar. 60, 9–19.

Lambert, C., Vidal, M., Penaud, A., Combourieu-Nebout, N., Lebreton, V., Ragueneau, O., Gregoire, G., 2017. Modern palynological record in the Bay of Brest (NW France): Signal calibration for palaeo-reconstructions. Rev. Palaeobot. Palynol. 244, 13–25. https://doi.org/10.1016/j.revpalbo.2017.04.005

Lambert, C., Penaud, A., Vidal, M., Klouch, K., Grégoire, G., Ehrold, A., Eynaud, F., Schmidt, S., Ragueneau, O., Sianno, R., 2018. Human-induced river runoff overlapping natural climate variability over the last 150 years: palynological evidence (Bay of Brest, NW France). Glob. Planet. Chang. 160, 109–122. https://doi.org/10.1016/j.gloplacha.2017.11.004

Lambert C., Vidal M., Penaud A., Le Roy P., Goubert E., Pailler Y., Stéphan P., Ehrhold A., 2019. Palaeoenvironmental reconstructions during the Meso- to Neolithic transition (9.2 – 5.3 cal ka BP) in Northwestern France: palynological evidences. Holocene 29, 380–402. https://doi.org/10.1177%2F0959683618816457

Lambert, C., Penaud, A., Vidal, M., Gandini, C., Labeyrie, L., Chauvaud, L., Ehrold, A., 2020. Striking forest revival at the end of the Roman Period in north-western Europe. Sci Rep 10, 21984. https://doi.org/10.1038/s41598-020-77253-1

Lambert, C., Penaud, A., Poirier, C., Goubert, E., 2022. Distribution of modern dinocysts in surface sediments of southern Brittany (NW France) in relation to environmental parameters: Implications for paleoreconstructions. Rev. of Palaeobot. and Palynol., 297, 104578. https://doi.org/10.1016/j.revpalbo.2021.104578

Lazure, P, Jégou, A.M., 1998. 3D modelling of seasonal evolution of Loire and Gironde plumes on Biscay Bay continental shelf. Oceanol. Acta. 21, 165–177. https://doi.org/10.1016/S0399-1784(98)80006-6

Lazure, P., Dumas, F., Vrignaud, C., 2008. Circulation on the Armorican shelf (Bay of Biscay) in autumn. J. Mar. Syst. 72, 218–237. https://doi.org/10.1016/j.jmarsys.2007.09.011

Lebreton, V., Messager, E., Marquer, L., Renault-Miskovsky, J., 2010. A neotaphonomic experiment in pollen oxidation and its implications for archaeopalynology. Rev. Palaeobot. Palynol., 162, 29–38. https://doi.org/10.1016/j.revpalbo.2010.05.002

Leorri, E., Cearreta, A., Milne, G., 2012a. Field observations and modelling of Holocene sea-level changes in the southern Bay of Biscay: implication for understanding current rates of relative sea-level change and vertical land motion along the Atlantic coast of SW Europe. Quat. Sci. Rev. 42, 59–73. https://doi.org/10.1016/j.quascirev.2012.03.014

Leorri, E., Fatela, F., Drago, T., Bradley, S.L., Moreno, J., Cearreta, A., 2012b. Lateglacial and Holocene coastal evolution in the Minho estuary (N Portugal): implications for understanding sea-level changes in Atlantic Iberia. Holocene 23, 353–363. https://doi.org/10.1177/0959683612460786

Le Roy, P., 2003. VIBARMOR cruise, RV Côtes De La Manche, https://doi.org/10.17600/3480160

Le Roy, P., Jouet, G., 2005. Remplissage sédimentaire meuble. In : Augris, C., Ménesguen, A., Hamon, D., Blanchet, A., Le Roy, P., Rolet, J., Jouet, G., Véron, G., Delannoy, H., 1081 Drogou, M., Bernard, C., Maillard, X., 2005. Atlas thématique de l'environnement marin de la Baie de Douarnenez. Ifremer (Ed), 61–72.

Lesueur, P., Klingebiel, A., 1986. Carte des sédiments superficiels du plateau continental du Golfe de Gascogne - Partie septentrionale au 1/500.000. Co-édition BRGM-Ifremer, carte géologique de la marge continentale française, 1carte, 1 notice, 23 p.

Lesueur, P., Jouanneau, J.-M., Boust, D., Tastet, J.P., Weber, O., 2001. Sedimentation rates and fluxes in the continental shelf mud fields in the Bay of Biscay (France). Cont. Shelf Res. 21, 1383–1401. https://doi.org/10.1016/S0278-4343(01)00004-8

Lohmann, K., Drange, H., Bentsen, M., 2009. Response of the North Atlantic subpolar gyre to persistent North Atlantic oscillation like forcing. Clim. Dyn. 32, 273–285. https://doi.org/10.1007/s00382-008-0467-6

Marguerie, D., 1990. L'environnement à l'Age du Fer en Armorique. In: Duval A, Le Bihan JP and Menez Y (eds) Les Gaulois d'Armorique: actes du 12e colloque de l'AFEAF, Quimper 1988 (Suppl Revue Archéologique de l'Ouest 3). Paris: Association Française pour l'Etude de 'l'Age du Fer, 115–120.

Marguerie, D., 1992. Évolution de la végétation sous l'impact humain en Armorique du Néolithique aux périodes historiques. Rennes, Travaux du Laboratoire d'Anthropologie de l'Université de Rennes 1, n° 40, 313 p.

Marguerie, D., 1993. Histoire de la végétation armoricaine. L'apport des restes végétaux des sites archéologiques et des tourbières. Penn ar Bed (Brest) 148-149, 32–45.

Marguerie, D., 2003. Bocages armoricains et sociétés, genèse, évolution et interactions. In: Des milieux et des hommes: fragments d'histoires croisés. Paris, Elsevier, 115–131.

Marret, F., Bradley, L., de Vernal, A., Hardy, W., Kim, S. Y., Mudie, P., Penaud, A., Pospelova, V., Price, A., Radi, T., Rochon, A., 2020. From bi-polar to regional distribution of modern dinoflagellate cysts, an overview of their biogeography. Mar. Micropaleontol., 159, 101753. https://doi.org/10.1016/j.marmicro.2019.101753

Mayewski, P.A., Rohling, E.E., Curt Stager, J., Karlén, W., Maasch, K.A., David Meeker, L., Meyerson, E.A., Gasse, F., Van Kreveld, S., Holmgren, K., Lee-Thorp, J., Rosqvist, G., Rack, F., Staubwasse, M., Schneider, R.R., Steig, E.J., 2004. Holocene climate variability. Quat. Res. 62, 243–255. https://doi.org/10.1016/j.yqres.2004.07.001

Mazier, F., Broström, A., Gaillard, M.-J., Sugita, S., Vittoz, P., and Buttier, A., 2008. Pollen productivity estimates and relevant source area of pollen for selected plant taxa in a pasture woodland landscape of the Jura Moutains (Switzerland). Veget. Hist. Archeobot., 17, 479–495. https://doi.org/10.1007/s00334-008-0143-0

Mazier, F., Broström, A., Bragée, P., Fredh, D., Stenberg, L., Thiere, G., Sugita, S., Hammarlund, D., 2015. Two hundred years of land-use change in the South Swedish Uplands: comparison of historical map-based estimates with a pollen-based reconstruction using the landscape reconstruction algorithm. Veg. Hist. Archaeobotany, 24, 555–570. https://doi.org/10.1007/s00334-015-0516-0

McCave, I.N., 1972. Transport and escape of fine-grained sediment from shelf areas. Shelf Sediment Transport, 225–248.

Menier, D., 2004. Morphologie et remplissage des vallées fossiles sud-armoricaines : Apport de la stratigraphie sismique. Mineralogy, Université Rennes 1, 202 p. https://tel.archives-ouvertes.fr/tel-00007291

Menier, D., Tessier, B., Proust, J.N., Baltzer, A., Sorrel, P., Traini, C., 2010. The Holocene transgression as recorded by incised valley infilling in a rocky coast context with low sediment supply (southern Brittany, western France). Bull. Géol. France 181, 2, 115–128. https://doi.org/10.2113/gssgfbull.181.2.115

Menier, D., Augris, C., Briend, C., 2014. Les réseaux fluviatiles anciens du plateau continental de Bretagne Sud. Editions Quae, 104 p.

Mertens, K.N., Verhoeven, K., Verleye, T., Louwye, S., Amorim, A., Ribeiro, S., et al., 2009. Determining the absolute abundance of dinoflagellate cysts in recent marine sediments: the *Lycopodium* marker-grain method put to the test. Rev. Palaeobot. Palynol. 157, 238–252. https://doi.org/10.1016/j.revpalbo.2009.05.004

Milne, G. A., Long, A.L., Basset, S.E., 2005. Modelling Holocene relative sea-level observations from the Caribbean and South Ameri. Quat. Sci Rev., 24, 1183–1202. https://doi.org/10.1016/j.quascirev.2004.10.005

Moffa-Sánchez, P., Hall, I.R., 2017. North Atlantic variability and its links to European climate over the last 3000 years. Nat Commun 8, 1726. https://doi.org/10.1038/s41467-017-01884-8

Mojtahid, M., Durand, M., Coste, P-O., Toucanne, S., Howa, H., Nizou, J., Eynaud, F., Penaud, A., 2019. Millennial-scale Holocene hydrological changes in the northeast Atlantic: New insights from '*La* Grande Vasière' mid-shelf mud belt. Holocene 29, 467–480. https://doi.org/10.1177/0959683618816478

Morley, A., Rosenthal, Y., Demenocal, P., 2014. Ocean-atmosphere climate shift during the mid-to-late Holocene transition. Earth Planet. Sci. Lett. 388, 18–26. https://doi.org/10.1016/j.epsl.2013.11.039

Morzadec-Kerfourn, M.-T., 1974. Variations de la ligne de rivage armoricaine au Quaternaire : analyses polliniques de dépôts organiques littoraux, Thèse, Université de Rennes 1, 208 p.

Morzadec-Kerfourn, M.-T., 1976. La signification écologique des dinoflagellés et leur intérêt pour l'étude des variations du niveau marin. Revue de Micropaléontologie 18, 229–235.

Morzadec-Kerfourn, M.-T., 1977. Les kystes de Dinoflagellés dans les sédiments récents le long des côtes bretonnes. Rev. de Micropaléontologie 20, 157–166.

Morzadec-Kerfourn, M.-T., 1992. Upper Pleistocene and Holocene dinoflagellate cyst assemblages in marine environments of the Mediterranean Sea and the north-west Atlantic coast of France. In: Head, M.J., and Wrenn, J.H. (eds.), Neogene and Quaternary Dinoflagellate Cysts and Acritarchs: American Association of Stratigraphic Palynologists Foundation, Dallas, 121–132.

Morzadec-Kerfourn, M.-T., 1997. Dinoflagellate cysts and the paleoenvironment of Late-Pliocene early-pleistocene deposits of Brittany, Northwest France. Quat. Sci. Revi. 16, 883–898.

Naughton, F., Bourillet, J.-F., Sanchez Goni, M.F., Turon, J.-L., Jouanneau, J.-M., 2007. Long-term and millennial-scale climate variability in northwestern France during the last 8850 years. Holocene 17, 939–953. https://doi.org/10.1177/0959683607082410

Olsen, J., Anderson, N.J., Knudsen, M.F., 2012. Variability of the Atlantic Oscillation over the past 5,200 years. Nat. Geosci. 5, 808–812. https://doi.org/10.1038/ngeo1589

Olsen, J.L., Mehlenbacher, S.A., Azarenko, A.N., 2000. Hazelnut Pollination. Hort. Technol., 10, 113–115. https://doi.org/10.21273/HORTTECH.10.1.113

Pailler, Y., Marchand, G., Blanchet, S., Guyodo, J.N., Hamon, G., 2008. Le Villeneuve-Saint-Germain dans la néolithisation de la péninsule armoricaine : les débuts d'une enquête, in L. Burnez-Lanotte, M. Ilett et P. Allard dir., Fin des traditions danubiennes dans le Néolithique du Bassin parisien et de la Belgique (5100-4700 BC), autour des recherches de Claude Constantin, Mémoire XLIV de la Société Préhistorique Française, Co-édition SPF et Presses Universitaire de Namur, 91–111.

Pailler, Y., Nicolas, C. dir., 2019. Une maison sous les dunes : Beg ar Loued, île Molène, Finistère. Identité et adaptation des groupes humains en mer d'Iroise à la transition des IIIe – IIe millénaires avant notre ère, Ed. Sidestone press, Leiden, 734 p.

Penaud, A., Ganne, A., Eynaud, F., Lambert, C., Coste, P.O., Herlédan, M., Vidal, M., Goslin, J., Stéphan, P., Charia, G., Pailler, Y., Durant, M., Zumaque, J., Mojtahid, M., 2020. Oceanic versus continental influences over the last 7 kyrs from a mid-shelf record in the northern Bay of Biscay (NE Atlantic). Quat.Sci. Rev. 229, 106135. https://doi.org/10.1016/j.quascirev.2019.106135

Perez-Belmonte, L., 2008. Caractérisation environnementale, morphosédimentaire et stratigraphique du Golfe du Morbihan pendant l'Holocène terminal : Implications Évolutives. Thèses, Université de Bretagne Sud. https://hal.archives-ouvertes.fr/tel-02382565

Pingree, RD, Le Cann, B, 1989. Celtic and Armorican slope and shelf residual currents. Prog. Oceanogr. 23, 303–338. https://doi.org/10.1016/0079-6611(89)90003-7

Proust, J.-N., Menier, D., Guillocheau, F., Guennoc, P., Bonnet, S., Le Corre, C., Rouby, D., 2001. Les vallées fossiles de la Vilaine : nature et évolution du prisme sédimentaire côtier du Pléistocène armoricain. – Bull. Soc. géol. Fr., 172, 6, 737-749. https://doi.org/10.2113/172.6.737

Puc, M., Kasprzyk, I., 2013. The patterns of *Corylus* and *Alnus* pollen seasons and pollination periods in two Polish cities located in different climatic regions. Aerobiologia 29, 495–511. https://doi.org/10.1007/s10453-013-9299-x

Reid, P.C., 1975. A regional sub-division of dinoflagellate cysts around the British Isles. The New Phytol. 75, 589–603. https://doi.org/10.1111/j.1469-8137.1975.tb01425.x

Reille, M., 1995. Pollen et spores d'Europe et d'Afrique du Nord: supplement 1. Laboratoire de Botanique Historique et Palynologie, Marseille, 327 p.

Reimer, P., Austin, W., Bard, E., Bayliss, A., et al., 2020. The IntCal20 Northern Hemisphere Radiocarbon Age Calibration Curve (0–55 cal kBP). Radiocarbon, 62(4), 725–757. https://doi.org/10.1017/RDC.2020.41

Rochon, A., Vernal, A.d., Turon, J.-L., Matthießen, J., Head, M., 1999. Distribution of recent dinoflagellate cysts in surface sediments from the North Atlantic Ocean and adjacent seas in relation to sea-surface parameters. American Association of Stratigraphic Palynologists Contribution Series. 35, 1–146.

Rodríguez-Rajo, F. J., Méndez, J., Jato, V., 2005. Environmental factors affecting pollination ecology of *Quercus* anemophilous species in North-West Spain. Bot. J. Linn. Soc., 15. https://doi.org/10.1111/j.1095-8339.2005.00460.x

Shom, 2012. PROTEUS_DUNES cruise, RV Pourquoi pas ?, https://doi.org/10.17600/12030130

Sjögren, P., van der Knaap, W.O., van Leeuwen, J.F., 2015. Pollen dispersal properties of Poaceae and Cyperaceae: First estimates of their absolute pollen productivities. Rev. Palaeobot. Palynol. 216, 123–131. https://doi.org/10.1016/j.revpalbo.2015.02.004

Stéphan, P., Goslin, J., Pailler, Y., Manceau, R., Suanez, S., Van Vliet-Lanoë, B., Hénaff, A., Delacourt, C., 2015. Holocene salt-marsh sedimentary infillings and relative sea-level changes in West Brittany (France) from foraminifera-based transfer functions. Boreas 44, 153–177. https://doi.org/10.1111/bor.12092

Stéphan, P., Verdin, F., Arnaud-Fassetta, G., Bertrand, F., Eynaud, F., García-Artola, A., Bosq, M., Culioli, C., Suanez, S., Coutelier, C., Bertran, P., Colin, A., Costa, S., 2019. Holocene coastal changes along the Gironde estuary (SW France): new insights from the North Medoc peninsula beach/dune system. Quaternaire 30, 47–75. https://doi.org/10.4000/quaternaire.11172

Stuiver, M., Reimer, P.J., 1993. Extended 14C database and revised CALIB radiocarbon calibration program. Radiocarbon 35, 215–230.

Tisnérat-Laborde, N., Paterne, M., Métivier, B., Arnold, M., Yiou, P., Blamart, D., Raynaud, S., 2010. Variability of the northeast Atlantic sea surface D14C and marine reservoir age and the North Atlantic Oscillation (NAO). Quat. Sci. Rev. 29. 2633–2646. https://doi.org/10.1016/j.quascirev.2010.06.013

Thornalley, D.J.R., Elderfield, H., McCave, I.N., 2009. Holocene oscillations in temperature and salinity of the surface subpolar North Atlantic. Nature 457, 711–714. https://doi.org/10.1038/nature07717

Tréguer, P., Goberville, E., Barrier, N., L'Helguen, S., Morin, P., Bozec, Y., Rimmelin-Maury, P., Czamanski, M., Grossteffan, E., Cariou, T., Répécaud, M., Quéméner, L., 2014. Large and local-scale influences on physical and chemical characteristics of coastal waters of Western Europe during winter. J. Mar. Syst. 139, 79–90. https://doi.org/10.1016/j.jmarsys.2014.05.019

Turon, J. L., 1984. Le palynoplancton dans l'environnement actuel de l'Atlantique Nord-oriental. Evolution climatique et hydrologique depuis le dernier maximum glaciaire. Mémoires de l'Institut de Géologie du Bassin d'Aquitaine 17, 313 pp.

van Beek, R., Marguerie, D., Bruel, F., 2018. Land use, settlement, and plant diversity in Iron Age Northwest France. Holocene, 28(4), 513–528. https://doi.org/10.1177/0959683617735590

Vanney, J.R., 1977. Géomorphologie de la marge continentale sud-armoricain. S.E.D.E.S, Paris, 473 p.

Van Nieuwenhove, N., Head, M. J., Limoges, A., Pospelova, V., Mertens, K. N., Matthiessen, J., De Schepper, S., de Vernal, A., Eynaud, F., Londeix, L., Marret, F., Penaud, A., Radi, T., Rochon, A., 2020. An Overview and Brief Description of Common Marine Organic-Walled Dinoflagellate Cyst Taxa

Occurring in Surface Sediments of the Northern Hemisphere. Mar. Micropaleontol. 159, 101814. https://doi.org/10.1016/j.marmicro.2019.101814

Visset, L., Sellier, D., L'Helgouach, J., 1995. Le paléoenvironnement de la région de Carnac. Sondage dans le marais de Kerdual, La Trinité-sur-Mer (Morbihan). IN : Revue archéologique de l'ouest, tome 12, 57–71. https://doi.org/10.3406/rao.1995.1025

Visset, L., L'Helgouach, J., Bernard, J., 1996. La tourbière submergée de la pointe de Kerpenhir à Locmariaquer (Morbihan). Etude environnementale et mise en évidence de déforestations et de pratiques agricoles néolithiques. Revue archéologique de l'ouest 13, 79–87. https://doi.org/10.3406/rao.1996.1041

Visset, L., Bernard, J., 2006. Evolution du littoral et du paysage, de la presqu'île de Rhuys à la rivière d'Etel (Massif armoricain – France), du Néolithique au Moyen Age. ArcheoSciences 30, 143–156. https://doi.org/10.4000/archeosciences.315

Wall, D., Dale, B., 1966. Living fossils in wester, Atlantic plankton. Nature 211 (5053), 1025–1026. https://doi.org/10.1038/2111025a0

Walker, KR., Bambach, R.K., 1971. The significance of fossil assemblages from fine-grained sediments: time-averaged communities. Abstracts with programs, Geol. Soc. Am. Annual Meeting, Washington. 783–784.

Walker, M., Gibbard, P., Head, M.J., Berkelhammer, M., Björck, S., Cheng, H., Cwynar, L.C., Fisher, D., Gkinis, V., Long, A., Lowe, J., Newnham, R., Rasmussen, S.O., Weiss, H., 2019. Formal Subdivision of the Holocene Series/Epoch: A Summary. J. Geo. Soc. India, 93, 135–141. https://doi.org/10.1007/s12594-019-1141-9

Weber, N., Chaumillon, E., Tesson, M., Garlan, T., 2004. Architecture and morphology of the outer segment of a mixed tide and wave-dominated incised valley, revealed by HR seismic reflection profiling: The paleo-Charente River, France. Mar. Geol., 207, 17-38. https://doi.org/10.1016/j.margeo.2004.04.001

Yonge, C., 1946. On the Habits of *Turritella Communis* Risso. Journal of the Marine Biological Association of the United Kingdom, 26(3), 377–380. https://doi.org/10.1017/S0025315400012194

Zonneveld, K.A., Marret, F., Versteegh, G.J., Bogus, K., Bonnet, S., Bouimetarhan, I., Crouch, E., de Vernal, A., Elshanawany, A., Edwards, L., Esper, O., Forke, S., Grøsfjeld, K., Henry, M., Holzwarth,

U., Kielt, J.F., Kim, S.Y., Ladouceur, S., Ledu, D., Chen, L., Limoges, A., Londeix, L., Lu, S.H., Mahmoud, M.S., Marino, G., Matsuoka, K., Matthiessen, J., Mildenhal, D.C., Mudie, P., Neil, H.L., Pospelova, V., Qi, Y., Radi, T., Richerol, T., Rochon, A., Sangiorgi, F., Solignac, S., Turon, J.L., Verleye, T., Wang, Y., Wang, Z., Young, M., 2013. Atlas of modern dinoflagellate cyst distribution based on 2405 data points. Rev. Palaeobot. Palynol. 191, 1–197. https://doi.org/10.1016/j.revpalbo.2012.08.003

Zumaque, J., Eynaud, F., de Vernal, A., 2017. Holocene paleoceanography of the Bay of Biscay: evidence for west-east linkages in the North Atlantic based on dinocyst data. Palaeogeogr. Palaeoclimatol. Palaeoecol. 468, 403–413. https://doi.org/10.1016/j.palaeo.2016.12.031